# Disentangling the pedogenic factors controlling active Al and Fe concentrations in soils of the Cameroon volcanic line

AUTHOR(S):

Watanabe, Tetsuhiro; Ueda, Shiori; Nakao, Atsushi; Ze, Antoine Mvondo; Dahlgren, Randy A.; Funakawa, Shinya

CITATION:

Watanabe, Tetsuhiro ...[et al]. Disentangling the pedogenic factors controlling active Al and Fe concentrations in soils of the Cameroon volcanic line. Geoderma 2023, 430: 116289.

ISSUE DATE:

2023-02

URL:

http://hdl.handle.net/2433/281878

Geoderma 430 (2023) 116289

Contents lists available at ScienceDirect

Geoderma

journal homepage: www.elsevier.com/locate/geoderma

# Disentangling the pedogenic factors controlling active Al and Fe concentrations in soils of the Cameroon volcanic line

Tetsuhiro Watanabe [a,b,*], Shiori Ueda [a], Atsushi Nakao [c], Antoine Mvondo Ze [d], Randy A. Dahlgren [e], Shinya Funakawa [a,b]

[a] Graduate School of Agriculture, Kyoto University, Kyoto 606-8502, Japan
[b] Graduate School of Global Environmental Studies, Kyoto University, Kyoto 606-8501, Japan
[c] Graduate School of Life and Environmental Sciences, Kyoto Prefectural University, Kyoto 606-8522, Japan
[d] Faculté d'Agronomie et des Sciences Agricoles, Université de Dschang, Dschang, Cameroon
[e] Department of Land, Air and Water Resources, University of California Davis, Davis, CA, 95616, USA

ARTICLE INFO

Handling Editor: Alberto Agnelli

*Keywords:*
Allophane
Gibbsite
Kaolinite
Andisol/Andosol

ABSTRACT

Active Al, Fe and Si (i.e., oxalate extractable fraction: $Al_o$, $Fe_o$, $Si_o$) strongly affect soil physical, chemical and biological properties. This study examined the pedogenic factors affecting $Al_o$, $Fe_o$ and $Si_o$ contents across a soil weathering sequence in the Cameroon volcanic line. We investigated the B horizon (~50-cm depth) from 26 soils formed in basaltic materials at different elevations (110–2570 m) incorporating a wide range of temperature (14–27 °C) and precipitation (1520–3130 mm). The weathering sequence ranged from weakly weathered Andisols in the southwest region grading to strongly weathered Oxisols on the central highlands. We assumed pyrophosphate extractable Al/Fe ($Al_p$/$Fe_p$) as organo-Al/Fe complexes, and $Si_o$, ($Al_o - Al_p$) and ($Fe_o - Fe_p$) as short-range-order (SRO) minerals. Factor analysis of climatic (e.g., temperature and precipitation/leaching metrics) and soil geochemical properties (e.g., weathering indices) identified three independent factors representing temperature/dry season intensity, weathering degree and precipitation/leaching as the primary determinants of $Al_o$, $Fe_o$ and $Si_o$ concentrations. Organo-metal complexes ($Al_p$ and $Fe_p$) were negatively correlated with the temperature/dry season intensity factor, whereas the SRO mineral phases ($Si_o$, $Al_o - Al_p$ and $Fe_o - Fe_p$) were negatively correlated with weathering degree. The precipitation/leaching factor positively correlated with $Al_o$, $Fe_o$ and $Si_o$. Our analysis infers that low temperature promotes the formation and preservation of organo-Al/Fe complexes, whereas weathering degree is more critical for SRO minerals. Further, increased weathering and a drier climate enhance the formation of crystalline clay minerals at the expense of SRO minerals. Allophanic materials ($Si_o$) were evident ($Si_o$: 9–43 g $kg^{-1}$) only in weakly weathered soils. However, low allophanic contents were found in more highly weathered soils ($Si_o$: 2–7 g $kg^{-1}$) accompanied by high $Al_p$ and $Fe_p$, suggesting the importance of volcanic parent materials as a direct source of Al and Fe via weathering for the formation of organo-metal complexes. In sum, we clarified the discriminatory effects of climatic factors and degree of weathering in regulating the composition of the active Al, Fe and Si fractions along the Cameroon volcanic line.

## 1. Introduction

Tephra as a soil parent material has a strong influence on soil properties, typically leading to the development of Andisols (Soil Survey Staff, 1999) or Andosols (IUSS Working Group WRB, 2015). Tephra deposits weather rapidly compared to their intrusive igneous counterparts owing to their considerable content of highly weatherable volcanic glass, and high surface area and porosity that facilitate rapid rock–water interactions. In turn, the rapid weathering leads to supersaturation of soil solutions with respect to several metastable short-range-order (SRO) minerals (Dahlgren et al. 2004). The distinctive characteristics of Andisols/Andosols derive predominantly from these SRO minerals (e.g., allophane, imogolite, ferrihydrite) and organo-Al/Fe complexes, which are collectively termed the active Al and Fe fraction and operationally defined as the acid oxalate extractable fraction ($Al_o$ and $Fe_o$). Although active Al and Fe in soils derived from tephra have significant importance in regulating soil properties, we find a distinct paucity of studies concerning their distribution in volcanic regions of tropical Africa.

* Corresponding author at: Graduate School of Agriculture, Kyoto University, Kyoto 606-8502, Japan.
*E-mail address:* watanabe.tetsuhiro.2m@kyoto-u.ac.jp (T. Watanabe).

https://doi.org/10.1016/j.geoderma.2022.116289
Received 13 May 2022; Received in revised form 20 November 2022; Accepted 25 November 2022
Available online 8 December 2022

The active Al and Fe fraction is highly reactive and contributes to a large phosphate adsorption capacity and a colloidal fraction dominated by variable charge characteristics. Furthermore, active Al and Fe components have a high affinity for organic matter interactions (e.g., sorption, complexation, physical protection in silt-sized aggregates), which results in the development of strong soil structure, low bulk density and a highly friable consistency (Asano and Wagai, 2014). Accordingly, a minimum value of 20 g $kg^{-1}$ of $Al_o + 1/2Fe_o$ is designated as one essential criterion for andic soil properties, which is necessary for the classification of Andisols/Andosols. However, even lower contents of active Al and Fe have an appreciable effect on soil properties leading to Soil Taxonomy defining andic subgroups for $Al_o + 1/2Fe_o$ contents >10 g $kg^{-1}$ (Soil Survey Staff, 2014). Moreover, even very low active Al and Fe contents in non-andic tropical soils are recognized to significantly control organic matter content (Ashida et al., 2021) and phosphate sorption capacity (Watanabe et al., 2015). Thus, active Al and Fe contents generally have a disproportionate importance on soil properties relative to their concentrations.

The active Al and Fe content varies considerably among soils owing primarily to differences in parent material, climate and age of soil. In general, higher active Al and Fe contents are found under stronger leaching conditions (Churchman and Lowe, 2012; Tsai et al., 2010), whereas more crystalline minerals (e.g., halloysite) tend to dominate under conditions of lower precipitation/leaching, which leads to a high silicic acid activity that favors halloysite formation over allophane and imogolite (Churchman and Lowe, 2012; Parfitt et al., 1983). Furthermore, higher temperature promotes the formation of crystalline minerals due to drier conditions that enhance evapotranspiration (Rasmussen et al., 2007; Schwertmann, 1985), lower levels of organic matter that inhibit crystallization of minerals (Huang et al., 2002; Schwertmann, 2008), and enhance dissolution/precipitation reactions resulting in transformation of metastable SRO minerals to more thermodynamically stable crystalline clays (i.e., Ostwald Ripening). In soils derived from tephra, the active Al and Fe fraction generally increases with soil development until intermediate stages when the most weatherable components (i.e., volcanic glass fraction) are depleted, and then tends to decrease as more crystalline aluminosilicates and Fe/Al (hydr) oxides are preferentially formed (Harsh et al., 2002; Torn et al., 1997). With progressive soil development, interactions between organic matter and minerals change from complexation of organic matter by active Al and Fe to surficial organic matter adsorption on crystalline secondary minerals (Chorover et al. 2004). Although some generalizations are possible, the specific combination of soil forming factors/processes controlling the active Al and Fe fraction is regional specific (e.g., tropical vs temperate vs boreal), which greatly complicates the development of a unifying theory for the pedogenesis of active Al and Fe components.

The Cameroon volcanic line in western Africa is characterized by a series of dominantly basaltic tephra deposits that increase in age from the southwest to northeast (Fig. 1). Also, climate conditions change with elevation, with higher elevation sites having lower temperatures, and hence lower evapotranspiration. Reflecting the age of volcanic activity and climate, Andosols were distributed near the coast and higher elevations of the inland area, whereas more weathered Cambisols, Nitisols and Ferralsols were found at lower elevations of the inland regions (Delvaux et al., 1989; Enang et al., 2021; Enang et al., 2020; Jones et al. 2013; Nakao et al., 2017; Proctor et al., 2007; Tematio et al., 2004; Van Ranst et al., 2019a). These trends in soil distribution suggest that the age of deposits and climate affect the occurrence and forms of active Al and Fe components. Previously, Van Ranst et al. (2019a) proposed that high active Al and Fe concentrations at high elevations (>1700 m) on Mount Bambouto were the result of organo-Al/Fe complexes formed from the dissolution of gibbsite and goethite, rather than direct weathering from volcanic ash. Notably, the relative importance of the factors/processes that control the active Al and Fe contents in soils of the Cameroon volcanic line has not been clearly elucidated, in part due to the narrow range of pedogenic factors (e.g., temperature, moisture and soil age) previously examined.

Herein, we aimed to clarify the primary factors affecting the active Al and Fe contents in soils along the Cameroon volcanic line. We collected 26 soils spanning a wide range of temperature (mean annual temperature [MAT]: 14–27 °C), moisture (mean annual precipitation [MAP]: 1520–3130 mm), and soil age (tephra deposits ranging in age from 0.01 to 11 Ma) from coastal areas to the central highlands at different elevations (110–2570 m). We hypothesized that soils with strongly contrasting pedogenic factors, especially temperature, moisture and soil age, would allow us to disentangle the interacting factors controlling the quantity and forms of active Al and Fe components.

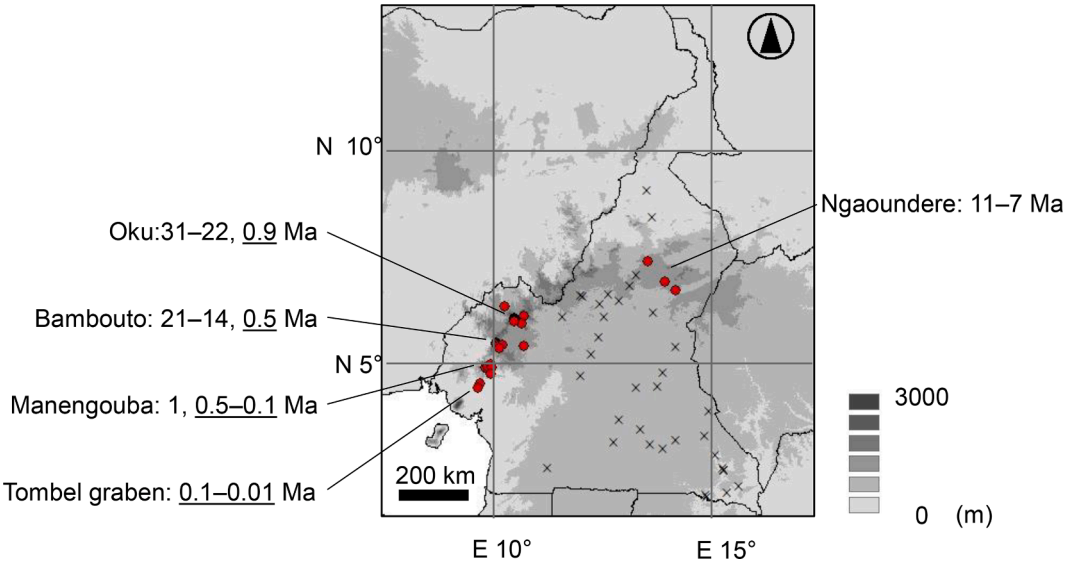


**Fig. 1.** Sampling sites (red circles) for soils investigated in this study on an elevation map of Cameroon. Sampling sites (cross) of other regional soils from the literature were used for comparison. Ages of the stratoid volcanism for Ngaoundere, Oku, Banbouto, and Manengouba from Marzoli et al. (2000) and ages of late-Quaternary volcanic activity for Oku, Banbouto, Manengouba, and Tombel graben (Dongmo et al., 2010) are shown without and with an underline, respectively. Mean annual temperature and precipitation values for the study area are shown in Fig. S1. (For interpretation of the references to colour in this figure legend, the reader is referred to the web version of this article.)

## 2. Materials and methods

### 2.1. Soil setting

The Cameroon volcanic line formed along a rift zone, and the volcanic deposits generally decrease in age from northeast to southwest: Mount Oku (31–22 Ma), Mount Bambouto (21–14 Ma), and Manengouba (1.55–0.11 Ma), with the exception of the Ngaoundere plateau (11–7 Ma; Enang et al., 2020; Marzoli et al., 2000). Tombel graben and Foumbot have experienced volcanic activity since the beginning of the Quaternary period (Delvaux et al., 1989). In the late-Quaternary, a number of basaltic eruptions were encountered from Mount Oku to Mount Cameroon (Dongmo et al., 2010). The late-Quaternary activity occurred 0.89 ± 0.10 Ma at Mount Oku, 0.48 ± 0.01 Ma at Mount Banbouto, 0.45 ± 0.04 to 0.11 ± 0.03 Ma at Mount Manengouba, and 0.12 ± 0.12 to 0.01 ± 0.11 at Tombel graben (Dongmo et al., 2010). Further, recent volcanic ash (~15000 BP) derived from the eastern edge of the Bamiléké plateau might cover the volcanic cone of Mount Bambouto (Van Ranst et al., 2019a citing Morin (1989)). Parent materials were mainly volcanic ejecta of basaltic composition (Nkouathio et al., 2008), with some alkali-rich volcanic materials (trachyte and phonolite; Marzoli et al., 2000; Nkouathio et al., 2008).

Soil temperature decreases with elevation resulting in soil temperature regimes from isohyperthermic to isothermic (Table 1, Fig. S1). Soil moisture regimes ranged between udic and ustic (Soil Survey Staff, 2014), showing regional differences rather than elevational gradients (Table 1, Fig. S1). The coastal region (Tombel graben and Manengouba) had higher precipitation compared to the central highlands (Ngaoundere plateau). Along elevational gradients (110–2570 m; Table 1), high elevation sites had lower temperatures, and hence lower evapotranspiration that led to higher excess precipitation (i.e., leaching). Vegetation cover shifts from dense evergreen forests near the coast to woodland/savanna vegetation at Mount Oku and Ngoundere plateau (Mayaux et al., 1999).

In the youngest regions (<0.1 Ma), Mount Cameroon and Tombel graben, soils contain high active Al and Fe contents that often meet andic soil property criteria (Delvaux et al., 1989; Proctor et al., 2007). In these soils, SRO minerals (e.g., allophane, imogolite and ferrihydrite) are found together with halloysite and kaolinite (Delvaux et al., 1989; Etame et al., 2009). In Mount Manengouba (0.5–0.1 Ma), silandic Andosols (i.e., dominated by allophanic minerals) were found at the summit (~2000 m), whereas aluandic (i.e., dominated by organo-Al complexes) Cambisols occurred at lower elevations (~1100 m; Enang et al., 2021; Enang et al., 2020). At Mount Banbouto (0.5 Ma), aluandic soils are found in the upper mountain (>2000 m), while aluandic-Ferralsols (1700–2000 m) and Ferralsols (1400–1600 m) dominate at lower elevations (Tematio et al., 2004; Van Ranst et al., 2019a). There is a paucity of pedological and mineralogical information for the older volcanic deposits located in the more interior regions of the Cameroon volcanic line (Mount Oku and Ngaoundere plateau), although highly weathered soils (Ferralsols) are found in the Adamawa plateau (Nakao et al., 2017), which includes the Ngaoundere plateau (7–11 Ma).

### 2.2. Soil samples and climate data

A total of 26 sites across the Cameroon volcanic line (110–2570 m) were selected to create a series of soils with contrasting parent material age and climate conditions (Table 1, Fig. 1, Fig. S1). All sites were composed of residual soils located on gentle upper slopes (<5%) near ridges or mid-slope positions (<5%). After a soil pedon was excavated to a depth of ~80 cm at each site (Fig. S2), soil samples were collected from three sides of each pedon, and a well-mixed composite sample was acquired for each horizon (Pennock et al., 2007). While soil samples were collected from the entire soil profile at each site, only soils from the B horizon (mostly the 40–60 cm depth) were fully characterized in this study to avoid alterations from human activities (e.g., land clearing and agriculture) that are more pronounced in the upper soil horizons. However, the A horizon soils were also evaluated for active Al and Fe (oxalate-extractable fraction) and SRO aluminosilicates (e.g., allophane/imogolite) for comparison purposes. Further, we compared our soils from the Cameroon volcanic line with soils from non-volcanic areas (mostly Oxisols and Ultisols) of Cameroon (Fig. 1) using data reported by Ashida et al. (2021) and Nakao et al. (2017) to determine if the effects of climate on active Al and Fe distributions were different between volcanic and non-volcanic soils. Parent materials of non-volcanic areas were Precambrian to Cambrian metamorphic rocks (e.g., schist, gneiss, quartzite, and migmatite), Precambrian plutonic rocks (e.g., granite, syenite, diorite, and gabbro), and Cretaceous sedimentary rocks (e.g., sandstone and limestone; Yerima and Van Ranst, 2005).

Climate data (mean annual/mean monthly temperature and precipitation based on 1950–2000 data) were obtained for each site from the WorldClim database (Hijmans et al., 2005). Potential evapotranspiration was estimated, following Thornthwaite (1948), from the monthly temperatures. Excess precipitation (EP) was calculated as precipitation minus potential evapotranspiration (Table 1) and used as an indicator of leaching intensity. Further, EP for the driest quarter of the year (EPDQ) was calculated and used as a metric of desiccation intensity during the dry season. Potential net primary production (NPP) was estimated using MAT and MAP values assuming tree-dominated systems (Del Grosso et al., 2008) and was considered as a proxy of organic matter input into soils.

### 2.3. Soil analysis

Each soil sample was air-dried and passed through a 2-mm sieve before further analysis. Soil pH was measured by mixing soil with deionized $H_2O$ at a soil:liquid ratio of 1:5 (g $mL^{-1}$) and measuring the pH after a 1-hr equilibration using a glass electrode. Total C content was determined by dry combustion using an elemental analyzer (Vario MAX, Elementar Analysensysteme); no carbonate minerals were present, so total carbon was assumed to be equal to organic C. Particle-size analysis was determined following organic matter removal by boiling 10 %

**Table 1**
Selected study site and soil taxonomy information.

| Region | Number of sites | Elevation | MAT | MAP | EP [a] | EP during driest quarter | NPP | Soil Taxonomy [b] |
|---|---|---|---|---|---|---|---|---|
| | | m | °C | mm | mm | mm | g C $m^{-2}$ $yr^{-1}$ | |
| Tombel graben | 2 | 110–390 | 25–27 | 3000–3130 | 1360–1740 | −280–−200 | 1025–1030 | Andisols (2) |
| Mount Manengouba | 6 | 690–1910 | 16–23 | 2150–2740 | 1300–1580 | −220–−100 | 924–1009 | Andisols (1), Inceptisols (3), Ultisols (2) |
| Mount Bambouto | 7 | 1520–2570 | 14–19 | 1930–2120 | 1050–1450 | −170–−80 | 825–925 | Andisols (1), Inceptisols (3), Ultisols (2), Oxisols (1) |
| Foumbot | 1 | 1220 | 21 | 1910 | 920 | −220 | 901 | Andisols (1) |
| Mount Oku | 7 | 730–2320 | 16–24 | 1900–2030 | 670–1260 | −290–−120 | 886–907 | Andisols (1), Inceptisols (2), Ultisols (4) |
| Ngaoundere plateau | 3 | 1120–1460 | 20–22 | 1520–1580 | 490–650 | −250–−210 | 787–804 | Oxisols (3) |

MAT: mean annual temperature, MAP: mean annual precipitation, EP: excess precipitation, NPP: net primary production.
[a] Mean annual precipitation minus potential evapotranspiration.
[b] Soil Survey Staff (2014).

$H_2O_2$, pH adjustment to 9–10 with 1 M NaOH solution or 5 with 1 M HCl solution when soil particles were not dispersed under alkaline conditions (pH 9–10), and ultrasonication for 15 min. The silt (2–20 μm) and clay (<2 μm) fractions were determined using the pipette method, whereas the coarse (0.2–2 mm) and fine (0.02–0.2 mm) sand fractions were determined by dry sieving (Gee and Or, 2002). Following clay/silt analysis, the clay fraction was isolated based on Stokes' law for mineralogical analyses. Exchangeable $Ca^{2+}$, $Mg^{2+}$, $K^+$ and $Na^+$ were extracted by 1 M $NH_4OAc$ at pH 7 (Soil Survey Staff, 1996) and quantified by atomic absorption spectroscopy for $Ca^{2+}$ and $Mg^{2+}$ and flame emission for $K^+$ and $Na^+$ (AA-660, Shimadzu). Cation exchange capacity was determined based on adsorbed $NH_4^+$ in the soil residue after exchangeable base extraction. Total elemental analysis of the <2-mm soil fraction was achieved by dissolution in aqua regia and HF (Hossner, 1996), with subsequent elemental quantification by inductively coupled plasma atomic emission spectrometry (ICP–AES; ICPE-9000, Shimadzu). The total Si to total (Al + Fe) ratio ($Si_t/(Al_t + Fe_t)$) and total reserve bases (TRB; defined as the sum of total Ca, Mg, K and Na contents) were calculated as weathering indices. The $Si_t/(Al_t + Fe_t)$ ratio is a measure of desilication, whereas TRB is a measure of the weatherable mineral content.

To estimate organo-Al/Fe complexes, SRO aluminosilicates and Fe (hydr)oxides fractions, we applied non-sequential, selective dissolution methods (Rennert, 2019; Shang and Zelazny, 2008). Pyrophosphate extractable Al and Fe ($Al_p$ and $Fe_p$) are considered as organically bound Al/Fe. Ammonium oxalate extractable Al, Fe and Si ($Al_o$, $Fe_o$ and $Si_o$) derive from SRO minerals (e.g., allophane/imogolite) and organically bound Al/Fe. We refer to $Al_o$ and $Fe_o$ as the active Al and Fe fraction, which is used as a criterion for andic soil properties in WRB and Soil Taxonomy. We assumed that ($Al_o - Al_p$) and ($Fe_o - Fe_p$) are derived predominantly from SRO minerals. Dithionite-citrate extracts free Fe (hydr)oxides (crystalline and SRO) and organically bound Fe. Because these operationally-defined methods are not completely selective (e.g., $Al_p$ and $Fe_p$ may include small particles of Al/Fe (hydr)oxides that are not bound to organic matter), we acknowledge that interpretation of extracted Al/Fe fractions includes inherent uncertainty (Rennert 2019). Selective dissolution followed Blakemore et al. (1987) using a sodium pyrophosphate (0.1 M, pH 10) for $Al_p$ and $Fe_p$, acidic ammonium oxalate (0.2 M, pH 3.0) in the dark for $Al_o$, $Fe_o$ and $Si_o$, and sodium dithionite-citrate for $Fe_d$. To minimize colloidal contamination of the pyrophosphate supernatant, we applied high-speed centrifugation (20,000 *g*) and filtration with a 0.025 μm filter as recommended by Schuppli et al. (1983). The Al, Fe and Si concentrations in pyrophosphate, ammonium oxalate, and dithionite-citrate extracts were determined by ICP-AES after passage through 0.025, 0.45 and 0.45 μm membrane filters, respectively. The content of the allophanic materials was calculated using the formula $Si_o \times 1.36\ ((Al_o - Al_p)/Si_o)^2 - 1.76\ ((Al_o - Al_p)/Si_o) + 5.44$) based on the data of Parfitt (1990). The content of ferrihydrite was calculated by multiplying the $Fe_o$ by 1.7 (Childs, 1985).

The crystalline mineral composition of the clay fraction was determined by X-ray diffraction (Miniflex 600, Rigaku) using Cu Kα radiation, a voltage of 40 kV and a current of 15 mA. An aliquot of the clay sample was saturated with $Mg^{2+}$, dried at 25 °C and analyzed by XRD with and without glycerol solvation. A second aliquot of clay was saturated with $K^+$ and subjected to XRD after heating/drying at 25, 350 and 550 °C (Harris and White, 2008). Peaks in X-ray diffractograms were classified as dominant (more than twice as high as other peaks), clear, unclear (approximately twice as high as the background noise), or not detected. Moreover, gibbsite and kaolin concentrations in each clay fraction were determined by differential thermal analysis (DTA) using a TA-60WS thermal analyzer (Shimadzu) equipped with a DTG60 simultaneous DTA–thermogravimetric (TG) apparatus (Shimadzu). DTA was performed at a heating rate of 20 °C $min^{-1}$ in a $N_2$ atmosphere. Iron (hydr) oxides were removed from each clay sample before DTA by treating the sample with a sodium dithionite–citrate solution (pH 7.3) at 80 °C. We used Al hydroxide (Wako) and Georgia kaolin (Nichika) as standards for gibbsite and kaolin, of which the calibration curves were confirmed by thermogravimetry.

### 2.4. Statistics

One-way analysis of variance and a Tukey-Kramer posthoc test were applied to assess differences in soil physicochemical properties among the five sampling regions. A Box-Cox transformation was applied when a parameter was not normally distributed as determined from a Shapiro–Wilk test. When a normal distribution was not achieved following transformation, an ANOVA using ranked order and Dunn's test were applied. Factor analysis was applied to simplify the climatic data (MAT, MAP, EP and EPDQ), weathering indices (TRB, $Si_t/(Al_t + Fe_t)$ and clay content), soil properties (total C), and potential NPP that were expected to affect the distribution of active Al and Fe and crystalline clay mineralogy. The relationship between factor scores, climatic data, and soil mineralogical and physicochemical properties (e.g., $Al_o$, $Fe_o$, $Si_o$, $Al_p$, $Fe_p$, $Fe_d$, gibbsite, and kaolin contents, pH) were investigated by Pearson's correlation analysis, where the Box-Cox transformation of parameters was applied when the parameter was not normally distributed. When a variable was not normally distributed after the Box-Cox transformation, Spearman's rank correlation analysis was applied. Finally, to assess potential relationships controlling the active Al and Fe fraction and soil mineralogical properties, variables representing various colloidal fractions were regressed with the factor scores using a generalized regression analysis with exponential distribution and a log-link function. Statistical analyses were performed using JMP Pro 15 (SAS Institute).

## 3. Results

### 3.1. Total elemental composition

Overall, the total elemental composition of the studied soils was generally low in Si and high in Fe (mean ± SD: 161 ± 33 g $kg^{-1}$ and 115 ± 26 g $kg^{-1}$, respectively) among igneous rock types and compared to the average composition of basalt (Si ≈ 234 g $kg^{-1}$ and Fe ≈ 83 g $kg^{-1}$ (Best, 2003); Table 2). A high Fe concentration was evident when compared to the non-volcanic soils in the region, which generally had <80 g Fe $kg^{-1}$ (Fig. S3). The young volcanic soils at Tombel graben and Foumbot tended to have higher total Si and base element (Ca, Mg, K, and Na) concentrations, but a lower Fe content, compared to the more highly weathered soils from Mount Bambouto, Mount Oku and Ngoundere plateau (Table 2), whereas the soils at Mount Manengouba were intermediate between these two groups. Correlations among total elemental concentrations showed an overall trend of Fe and Al being negatively correlated with Si, Ca, Mg and K (Table S1), consistent with an enrichment of Al and Fe versus depletion of Si and base elements upon increasing chemical weathering.

### 3.2. Physicochemical soil properties

Total C content of B horizons ranged from 6 to 65 g $kg^{-1}$ (Table 3 and Table S2) and was negatively correlated with MAT ($rs = -0.56$, $P < 0.01$; Fig. S4). Soil pH was slightly acidic (6.0–6.5) at Foumbot and Tombel graben (youngest soils) to extremely acidic at Ngaoundere plateau (4.4–4.5; oldest soils). The clay content was generally high (>30 %) except for the young Andisols from Tombel graben (Table 3 and Table S2). Clay content was negatively correlated with TRB ($rs = -0.72$, $P < 0.001$), while the sand content was positively correlated with TRB and $Si_t/(Al_t + Fe_t)$ ($rs = 0.48$, $P < 0.05$, and $rs = 0.47P < 0.05$, respectively; Fig. S4). Soil pH did not reflect climatic conditions, such as MAP and EP, but rather was more strongly affected by the weathering degree as reflected by TRB ($rs = 0.64$, $P < 0.001$) and clay content ($rs = -0.49$, $P < 0.05$). Exchangeable bases had a strong correlation with pH ($rs = 0.70$, $P < 0.001$) and were low in soils with low TRB ($rs = 0.51$, $P <$

**Table 2**
Total elemental contents (mean ± standard deviation) and weathering indices of B horizons in each region and an idealized unweathered basalt. Different letters after values indicate mean values are significantly different between regions.

| Region | Si | | Al | | Fe | | Ca [a] | | Mg [a] | | K [a] | | Na [a] | | TRB [b] | | $Si_t/(Al_t + Fe_t)$ [a] | |
|---|---|---|---|---|---|---|---|---|---|---|---|---|---|---|---|---|---|---|
| | ($g\ kg^{-1}$) | | | | | | | | | | | | | | ($cmol_c\ kg^{-1}$) | | (mol/mol) | |
| Foumbot & Tombel graben | 194 | ±16 | 100 | ±24 | bc | 102 | ±29 | 23 | ±11 | a | 30.3 | ±14.1 | a | 8.2 | ±6.0 | 11 | ±10 | 432 | ±182 | a | 1.34 | ±0.52 |
| Mount Manengouba | 181 | ±37 | 136 | ±17 | ab | 104 | ±14 | 3.0 | ±5.4 | ab | 8.2 | ±12.1 | ab | 3.6 | ±1.4 | 5.3 | ±3.9 | 115 | ±129 | ab | 0.94 | ±0.20 |
| Mount Bambouto | 146 | ±16 | 172 | ±23 | a | 108 | ±29 | 1.0 | ±1.2 | ab | 2.6 | ±1.4 | bc | 2.6 | ±1.9 | 3.5 | ±1.6 | 48 | ±15 | bc | 0.64 | ±0.12 |
| Mount Oku | 152 | ±37 | 152 | ±28 | a | 124 | ±23 | 0.8 | ±0.7 | bc | 4.1 | ±2.8 | ab | 2.6 | ±2.0 | 5.2 | ±3.6 | 66 | ±25 | ab | 0.72 | ±0.29 |
| Ngaoundere plateau | 144 | ±22 | 149 | ±16 | ab | 144 | ±26 | 0.4 | ±0.4 | bc | 2.5 | ±1.8 | bc | 1.5 | ±0.6 | 3.3 | ±1.9 | 41 | ±14 | bc | 0.64 | ±0.15 |
| ANOVA [c] | N.S. | | $P < 0.01$ | | N.S. | | $P < 0.05$ | | $P < 0.05$ | | N.S. | | N.S. | | $P < 0.05$ | | $P < 0.05$ | |
| Basalt [d] | 234 | | 85 | | 83 | | 69 | | 41 | | 9.3 | | 22 | | 802 | | 1.80 | |

[a] Box-Cox transformation was applied before ANOVA and the multiple comparisons.
[b] Dunn's test was applied for multiple comparisons.
[c] ANOVA: analysis of variance, N.S.: not significant ($P \geq 0.05$).
[d] Average chemical composition of basalt from all over the world ($n = 3594$; Best, 2003).

0.001).

### 3.3. Climate and weathering conditions

Factor analysis using climate data, weathering indices, total C and potential NPP yielded three factors, which explained 87 % of the total variation (Table 4). The first factor (37.5 % contribution) had a high positive loading with MAT, and high negative loadings with EPDQ and total C. In contrast to EPDQ, EP did not show a high contribution to the first factor. We interpret the first factor to dominantly represent a temperature and desiccation intensity driver in which higher temperatures decrease total C. The second factor (32.6 % contribution) showed positive loadings with MAP, EP and NPP, which was mainly controlled by precipitation across our sampling sites. We interpret the second factor to represent precipitation and leaching intensity. The third factor (16.5 % contribution) had a negative loading with TRB and $Si_t/(Al_t + Fe_t)$ and a positive loading with clay content, thereby being indicative of a degree of weathering factor. The three factors were not correlated with each other and were therefore considered to be independent factors.

The score of factor 1 (temperature/desiccation) was low for the soils at high elevations (Fig. 2a), where desiccation during the dry season is less distinct and organic matter tends to accumulate. The precipitation/leaching intensity associated with factor 2 clearly reflected the trend of decreased rainfall/leaching from the coastal region (Tombel graben) to the inland sites (Ngaoundere plateau; Fig. 2b and Fig. S1). The weathering degree indicated by factor 3 was low for the younger soils from Tombel graben and Foumbot (Fig. 2a), which contained observable weathered scoria in the soil profiles. The other soils showed higher factor 3 weathering scores, although the older soils from Mount Oku had somewhat lower values, probably reflecting the drier climate that tends to limit weathering and conserve total bases (TRB). Weathering is generally enhanced by high temperature and precipitation, but such relationships between weathering indices (TRB, $Si_t/(Al_t + Fe_t)$ and clay content) and temperature or moisture were not found in the studied soils (Fig. S4).

### 3.4. Selective dissolution

The $Al_o$, $Fe_o$ and $Si_o$ contents showed a wide range of values for the B horizons (3.2–83.0, 3.2–57.1 and 0.1–43.1 g $kg^{-1}$, respectively; Table 5). High values of $Al_o$, $Fe_o$ and $Si_o$ were found in the young volcanic soils (Foumbot and Tombel graben) and soils with low MAT (<~20 °C) at higher elevations (>~2000 m) of the other volcanic regions (Manengouba, Banbouto, and Oku). The $Al_o$ content decreased with temperature/desiccation intensity (Factor 1; $r = -0.60$, $P < 0.01$) and weathering degree (Factor 3; $r = -0.54$, $P < 0.01$), but increased with moisture/leaching (Factor 2; $r = 0.43$, $P < 0.05$; Table 6). The $Fe_o$ and $Si_o$ contents showed similar trends and were correlated with temperature/desiccation intensity, weathering degree and precipitation/leaching factor scores, except there was no correlation between $Si_o$ and the temperature/desiccation factor (Table 6). The regression analysis also inferred significant roles for temperature, weathering degree and precipitation/leaching in regulating the oxalate-extractable components, although the coefficient for precipitation/leaching factor was not significant for $Al_o$ (Table 7).

The $Al_o$, $Fe_o$ and $Si_o$ contents in A horizons showed a similar trend to their corresponding B horizons (Fig. S5), that is, when the B horizons had high values of $Al_o$, $Fe_o$ and $Si_o$, the A horizon also had high values. A decreasing trend for $Al_o$ with increasing temperature was also found for the non-volcanic soils outside of the study regions ($r_s = -0.33$, $P < 0.05$), but the $Al_o$ values were relatively low (<6 g $kg^{-1}$). Conversely, $Fe_o$ and $Si_o$ contents did not show a significant correlation with temperature for the non-volcanic soils (Fig. S6).

Organically bound Al/Fe ($Al_p$ and $Fe_p$) and SRO minerals ($Si_o$, $Al_o - Al_p$ and $Fe_o - Fe_p$) showed different trends with respect to correlations with the factor scores. The $Al_p$ and $Fe_p$ were negatively correlated with

**Table 3**
Selected physicochemical properties of B horizons. Different letters after values indicate values are significantly different between regions.

| Region | n | Total C [a] | | Sand [a] | | | Silt [b] | | Clay [b] | | pH($H_2O$) [a] | | | Exch. bases [a] | | | CEC | | |
|---|---|---|---|---|---|---|---|---|---|---|---|---|---|---|---|---|---|---|---|
| | | (g $kg^{-1}$) | | (%) | | | (%) | | (%) | | | | | ($cmol_c$ $kg^{-1}$) | | | ($cmol_c$ $kg^{-1}$) | | |
| Foumbot & Tombel graben | 3 | 22 | ±9 | 36 | ±19 | a | 38 | ±8 | 26 | ±14 | 6.3 | ±0.3 | a | 14.2 | ±7.2 | a | 26.3 | ±2.2 | ab |
| Mount Manengouba | 6 | 18 | ±21 | 13 | ±10 | ab | 29 | ±18 | 58 | ±22 | 5.1 | ±1.0 | bc | 3.5 | ±4.0 | bc | 28.6 | ±5.4 | a |
| Mount Bambouto | 7 | 30 | ±23 | 4 | ±1 | bc | 40 | ±29 | 56 | ±30 | 5.6 | ±0.2 | ab | 4.7 | ±4.4 | ab | 19.9 | ±5.4 | bc |
| Mount Oku | 7 | 26 | ±18 | 10 | ±9 | ab | 38 | ±18 | 51 | ±16 | 5.4 | ±0.4 | ab | 1.8 | ±1.4 | bc | 17.3 | ±6.6 | bc |
| Ngaoundere plateau | 3 | 15 | ±1 | 5 | ±6 | bc | 18 | ±2 | 76 | ±7 | 4.4 | ±0.1 | bc | 0.6 | ±0.4 | c | 8.2 | ±2.6 | c |
| ANOVA [c] | | N.S. | | $P < 0.01$ | | | N.S. | | N.S. | | $P < 0.01$ | | | $P < 0.001$ | | | $P < 0.001$ | | |

[a] Box-Cox transformation was applied before ANOVA and the multiple comparisons.
[b] Analysis of variance in rank order was applied.
[c] Analysis of variance in rank order was applied.

**Table 4**
Factor analysis of climate data, weathering indices and soil properties.

| | Factor-1 | Factor-2 | Factor-3 |
|---|---|---|---|
| MAT | 0.87 | 0.21 | −0.33 |
| MAP | 0.17 | 0.95 | −0.25 |
| EP | −0.48 | 0.87 | −0.10 |
| EP in driest quarter | −0.98 | 0.07 | 0.02 |
| TRB | −0.06 | 0.20 | −0.84 |
| $Si_t/(Al_t + Fe_t)$ | 0.20 | 0.12 | −0.64 |
| Clay | 0.44 | −0.18 | 0.66 |
| Total C | −0.70 | −0.02 | −0.25 |
| NPP | 0.19 | 0.90 | −0.19 |
| Eigenvalue | 3.38 | 2.94 | 1.48 |
| Contribution % | 37.5 | 32.6 | 16.5 |

MAT: mean annual temperature, MAP: mean annual precipitation, EP: excess precipitation, TRB: total reserve bases, $Si_t/(Al_t + Fe_t)$: ratio of total Si to total Al plus Fe, NPP: net primary production.

the temperature/desiccation intensity (Factor 1; Fig. 3), a factor that also included a loading contribution from organic C. In contrast, $Si_o$, $Al_o - Al_p$ and $Fe_o - Fe_p$ were correlated with weathering degree (Factor 3; Table 6, Fig. 3). The magnitude of correlation coefficients in the regression equations further supported that temperature was an important factor determining $Al_p$ and $Fe_p$ contents, and weathering degree was more important for regulating SRO minerals than temperature (Table 7). Total C content showed a stronger relationship with $Al_p$ and $Fe_p$ ($r_s = 0.73$, $P < 0.001$ and $r_s = 0.53$, $P < 0.01$, respectively) than $Al_o$ and $Fe_o$ ($r_s = 0.61$, $P < 0.001$ and $r_s = 0.29$, $P = 0.14$, respectively; Fig. S4).

The $Fe_d$ content was generally high, mostly exceeding 70 g $kg^{-1}$ (Table 5), and increased with the weathering degree (Table 6). The crystallinity of Fe (hydr)oxides increased with weathering and temperature, and $Fe_o/Fe_d$ was negatively correlated with the weathering factor (Factor 3) and positively correlated with the precipitation/leaching factor (Factor 2). Although $Fe_o/Fe_d$ appeared higher at high elevations in each region (Table 5), it did not correlate with the temperature/desiccation factor (Factor 1; Table 6). The correlation coefficients of the regression analysis showed negative contributions from the temperature/desiccation and weathering factors and a positive contribution of the precipitation/leaching factor to $Fe_o/Fe_d$ (Table 7). A positive correlation between the ratio of organo-Al to $Al_o$, $Al_p/Al_o$ and the weathering factor (Factor 3; $r = 0.46$, $P < 0.05$) suggests that the organo-Al fraction increases with weathering (Table 6). On the other hand, the frequently observed negative relationship between pH and $Al_p/Al_o$ (Takahashi and Dahlgren, 2016) was not significant in the studied soils (Fig. S4). The Si-to-Al ratio of SRO minerals, $Si_o/(Al_o - Al_p)$, was higher for less weathered soils (Table 6).

Among the extracted components, the $Si_o$ content was strongly correlated with SRO Al and Fe phases ($Al_o - Al_p$: $rs = 0.81$, $P < 0.001$; $Fe_o - Fe_p$: $rs = 0.81$, $P < 0.001$) and was moderately correlated with organo-Al/Fe ($Al_p$: $rs = 0.68$, $P < 0.001$; $Fe_p$: $rs = 0.42$, $P < 0.05$). Additionally, the $Si_o/(Al_o - Al_p)$ ratio of most soils was close to 0.5,

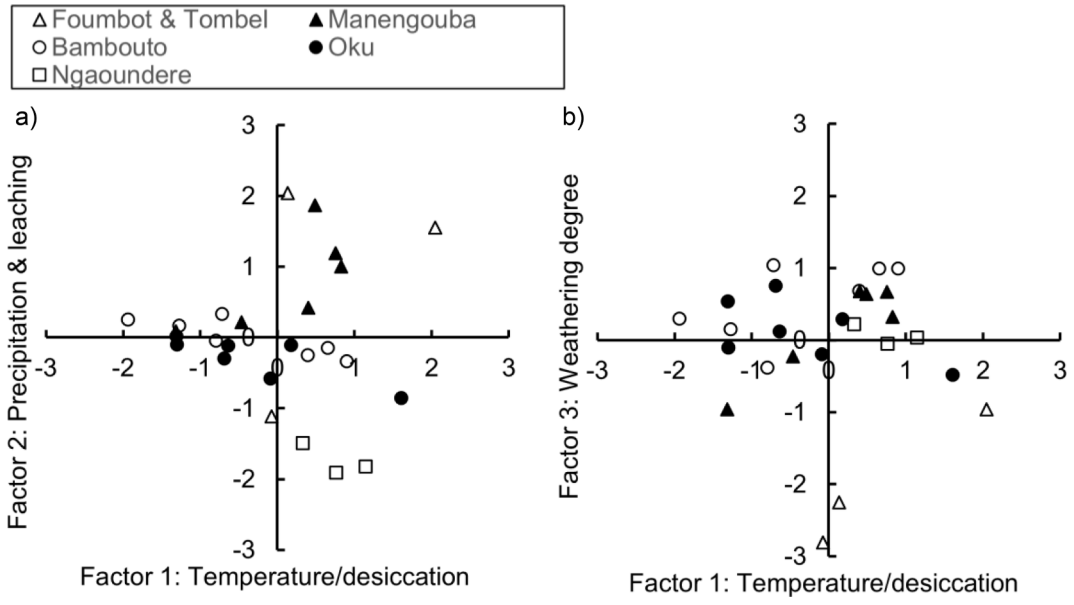


**Fig. 2.** Factor scores representing temperature/dry season desiccation intensity (factor 1), precipitation/leaching (factor 2) and weathering degree (factor 3) for B horizons.

**Table 5**
Mineralogical properties of B horizons based on selective dissolution.

| Site | $Al_o$ | $Fe_o$ | $Si_o$ | $Al_p$ | $Fe_p$ | $Fe_d$ | $Al_o + 1/2Fe_o$ | $Al_o - Al_p$ | $Fe_o - Fe_p$ | $Fe_o/Fe_d$ | $Al_p/Al_o$ | $Si_o/(Al_o - Al_p)$ |
|---|---|---|---|---|---|---|---|---|---|---|---|---|
| | g kg$^{-1}$ | | | | | | | | | (mol mol$^{-1}$) | | |
| Foumbot & Tombel graben | | | | | | | | | | | | |
| F1 | 21.2 | 20.7 | 14.2 | 3.5 | 2.1 | 31.4 | 31.5 | 17.7 | 18.6 | 0.66 | 0.17 | 0.80 |
| T1 | 71.8 | 50.0 | 43.1 | 5.0 | 2.5 | 80.5 | 96.8 | 66.8 | 47.4 | 0.62 | 0.07 | 0.65 |
| T2 | 17.5 | 27.3 | 9.4 | 2.1 | 2.1 | 87.7 | 31.1 | 15.4 | 25.1 | 0.31 | 0.12 | 0.61 |
| Mount Manengouba | | | | | | | | | | | | |
| M1 | 83.0 | 57.1 | 32.6 | 14.9 | 13.0 | 86.9 | 112 | 68.1 | 44.1 | 0.66 | 0.18 | 0.48 |
| M2 | 10.1 | 24.4 | 3.6 | 1.9 | 2.5 | 63.5 | 22.3 | 8.3 | 21.9 | 0.38 | 0.19 | 0.43 |
| M3 | 5.6 | 8.8 | 0.9 | 1.8 | 3.1 | 58.8 | 10.0 | 3.9 | 5.7 | 0.15 | 0.31 | 0.24 |
| M4 | 9.1 | 17.3 | 0.6 | 1.3 | 1.4 | 68.7 | 17.7 | 7.8 | 15.9 | 0.25 | 0.14 | 0.07 |
| M5 | 5.6 | 9.4 | 0.7 | 2.1 | 3.0 | 85.6 | 10.3 | 3.5 | 6.3 | 0.11 | 0.37 | 0.20 |
| M6 | 4.6 | 4.5 | 0.5 | 2.1 | 4.6 | 86.6 | 6.9 | 2.5 | <0.1 | 0.05 | 0.45 | 0.21 |
| Mount Bambouto | | | | | | | | | | | | |
| B1 | 25.9 | 22.1 | 6.0 | 5.5 | 2.7 | 71.0 | 36.9 | 20.4 | 19.4 | 0.31 | 0.21 | 0.30 |
| B2 | 27.5 | 22.3 | 4.1 | 15.1 | 14.3 | 106 | 38.6 | 12.4 | 7.9 | 0.21 | 0.55 | 0.33 |
| B3 | 7.3 | 6.6 | 0.3 | 3.3 | 6.3 | 102 | 10.6 | 4.0 | 0.3 | 0.06 | 0.45 | 0.08 |
| B4 | 21.4 | 8.8 | 5.8 | 6.8 | 3.4 | 78.1 | 25.8 | 14.6 | 5.4 | 0.11 | 0.32 | 0.40 |
| B5 | 3.7 | 3.8 | 0.4 | 0.7 | 1.1 | 106 | 5.6 | 3.0 | 2.8 | 0.04 | 0.18 | 0.15 |
| B6 | 3.5 | 6.8 | 0.4 | 0.5 | 1.0 | 138 | 6.9 | 3.0 | 5.8 | 0.05 | 0.15 | 0.15 |
| B7 | 5.0 | 3.6 | 0.3 | 1.0 | 1.9 | 71.6 | 6.8 | 3.9 | 1.7 | 0.05 | 0.21 | 0.08 |
| Mount Oku | | | | | | | | | | | | |
| O1 | 12.0 | 20.0 | 0.6 | 11.6 | 24.7 | 91.8 | 22.1 | 0.4 | <0.1 | 0.22 | 0.97 | 1.48 |
| O2 | 35.3 | 22.3 | 6.5 | 14.8 | 10.4 | 78.3 | 46.5 | 20.5 | 11.9 | 0.28 | 0.42 | 0.32 |
| O3 | 6.6 | 6.5 | 0.2 | 2.9 | 4.8 | 125 | 9.8 | 3.6 | 1.7 | 0.05 | 0.45 | 0.04 |
| O4 | 18.9 | 19.3 | 2.4 | 9.0 | 10.9 | 99.3 | 28.6 | 9.9 | 8.4 | 0.19 | 0.48 | 0.24 |
| O5 | 4.2 | 4.8 | 0.2 | 0.9 | 1.1 | 99.3 | 6.6 | 3.4 | 3.8 | 0.05 | 0.21 | 0.07 |
| O6 | 6.9 | 12.6 | 1.0 | 2.2 | 2.7 | 96.7 | 13.2 | 4.8 | 9.9 | 0.13 | 0.32 | 0.21 |
| O7 | 3.7 | 6.1 | 0.5 | 1.4 | 2.3 | 65.2 | 6.8 | 2.3 | 3.8 | 0.09 | 0.39 | 0.21 |
| Ngaoundere plateau | | | | | | | | | | | | |
| N1 | 3.7 | 4.0 | 0.1 | 1.0 | 1.3 | 91.5 | 5.7 | 2.8 | 2.7 | 0.04 | 0.26 | 0.04 |
| N2 | 3.8 | 3.3 | 0.4 | 0.7 | 0.3 | 83.1 | 5.4 | 3.1 | 3.0 | 0.04 | 0.19 | 0.12 |
| N3 | 3.2 | 3.2 | 0.2 | 1.0 | 1.1 | 91.8 | 4.7 | 2.2 | 2.0 | 0.03 | 0.31 | 0.08 |

$Al_o$, $Fe_o$, $Si_o$: acid oxalate extractable Al, Fe, Si; $Al_p$, $Fe_p$: pyrophosphate extractable Al, Fe; $Fe_d$: Dithionite-citrate extractable Fe.
$Al_o - Al_p$ and $Fe_o - Fe_p$ are derived predominantly from short-range-order minerals. $Fe_o/Fe_d$ is an index of Fe (hydr)oxide activity. $Al_p/Al_o$ indicates organo-Al contribution to active Al fraction. $Si_o/(Al_o - Al_p)$ is the Si to Al ratio in short-range-order aluminosilicates, namely allophane and/or imogolite.

**Table 6**
Pearson correlation coefficients between factor scores and mineralogical properties.

| | Factor 1 | | Factor 2 | | Factor 3 | |
|---|---|---|---|---|---|---|
| | Temperature & dry season desiccation intensity | | Precipitation & leaching | | Weathering degree | |
| $Al_o$ | −0.60 | ** | 0.43 | * | −0.54 | ** |
| $Fe_o$ | −0.46 | * | 0.50 | ** | −0.55 | ** |
| $Si_o$ | −0.35 | | 0.45 | * | −0.66 | *** |
| $Al_p$ | −0.72 | *** | 0.32 | | −0.31 | |
| $Fe_p$ | −0.64 | *** | 0.37 | | 0.02 | |
| $Fe_d$ | −0.09 | | −0.01 | | 0.47 | * |
| $Al_o - Al_p$ | −0.28 | | 0.33 | | −0.62 | *** |
| $Fe_o - Fe_p$ | −0.08 | | 0.22 | | −0.68 | *** |
| $Fe_o/Fe_d$ | −0.39 | | 0.44 | * | −0.63 | *** |
| $Al_p/Al_o$ | −0.37 | | −0.15 | | 0.46 | * |
| $Si_o/(Al_o - Al_p)$ | −0.28 | | 0.36 | | −0.54 | ** |
| Kaolin | 0.63 | *** | 0.06 | | 0.13 | |
| Gibbsite | −0.40 | * | −0.50 | ** | 0.37 | |
| Gibbsite/kaolin | −0.65 | *** | −0.39 | * | 0.13 | |

*: $P < 0.05$, **: $P < 0.01$, *: $P < 0.001$.
$Al_o$, $Fe_o$, $Si_o$: acid oxalate extractable Al, Fe, Si; $Al_p$, $Fe_p$: pyrophosphate extractable Al, Fe; $Fe_d$: Dithionite-citrate extractable Fe.
$Al_o - Al_p$ and $Fe_o - Fe_p$ are derived predominantly from short-range-order minerals. $Fe_o/Fe_d$ is an index of Fe oxide activity. $Al_p/Al_o$ indicates organo-Al contribution to active Al fraction. $Si_o/(Al_o - Al_p)$ is the Si to Al ratio in short-range-order aluminosilicates, namely allophane and/or imogolite. Kaolin and gibbsite contents were determined by DTA.

which is the theoretical ratio for imogolite and low Si (Al-rich) allophane (Fig. 4). Elevated $Si_o$ content and the $Si_o/(Al_o - Al_p)$ of 0.5 infer the presence of SRO aluminosilicates, such as allophane and imogolite. High values of $Al_o - Al_p$, as well as $Al_o$ and $Fe_o$, were found in the soils with $Si_o$ values of >2 g kg$^{-1}$ (Table 5, Fig. 4). Free Fe (hydr)oxides extracted by dithionite-citrate ($Fe_d$) showed no significant correlation with $Fe_o$ or $Fe_p$ (Fig. S4).

### 3.5. X-ray diffraction and differential thermal analyses of clay fraction

X-ray diffraction and DTA showed that kaolin minerals and gibbsite were the dominant crystalline clay minerals in the B horizons (Table 8). The kaolin minerals were dominated by 0.7 nm kaolinite forms, whereas 1.0 nm hydrated halloysite was found at low levels in only two soils. The soils in the young volcanic area (Foumbot and Tombel graben) and those at Mount Manengouba had more kaolin minerals than gibbsite, whereas the other volcanic regions had moderate concentrations of both minerals. Temperature/desiccation intensity (Factor1) was positively correlated with kaolin content and negatively correlated with gibbsite content (Table 6). At Mount Bambouto and Mount Oku, more kaolin minerals relative to gibbsite were found at lower elevations (Table 8). The higher content of kaolin minerals versus gibbsite at lower elevations was reflected in the positive correlation of kaolin content and negative correlation of gibbsite and the gibbsite/kaolin ratio with the temperature/desiccation intensity factor (Table 6). Additionally, gibbsite content was negatively correlated with the precipitation/leaching factor (Table 6). Hydroxy-Al interlayered vermiculite and quartz were widely distributed at low levels across the study area. Kaolin mineral contents determined by DTA were negatively correlated with $Al_o$ and $Al_p$ ($r$ =

**Table 7**
Generalized linear regression analysis using factor scores representing temperature and dry season desiccation intensity (FS1), precipitation/leaching (FS2) and weathering degree (FS3).

| Mineralogical Parameter | | Constant | Coefficient FS1 | | Coefficient FS2 | | Coefficient FS3 | |
|---|---|---|---|---|---|---|---|---|
| log $Al_o$ (g $kg^{-1}$) | = | 2.41 | −0.53 | × FS1 | | | −0.74 | × FS3 |
| log $Fe_o$ (g $kg^{-1}$) | = | 2.45 | −0.40 | × FS1 | +0.46 | × FS2 | −0.52 | × FS3 |
| log $Si_o$ (g $kg^{-1}$) | = | 0.47 | −0.64 | × FS1 | +0.69 | × FS2 | −1.32 | × FS3 |
| log $Al_p$ (g $kg^{-1}$) | = | 1.17 | −0.72 | × FS1 | | | | |
| log $Fe_p$ (g $kg^{-1}$) | = | 1.32 | −0.67 | × FS1 | | | | |
| log ($Al_o$ − $Al_p$) (g $kg^{-1}$) | = | 2.04 | −0.42 | × FS1 | | | −0.86 | × FS3 |
| log ($Fe_o$ − $Fe_p$) (g $kg^{-1}$) | = | 2.08 | | | | | −0.87 | × FS3 |
| log ($Fe_o$/$Fe_d$) | = | −1.95 | −0.38 | × FS1 | +0.45 | × FS2 | −0.69 | × FS3 |
| log Kaolin (g $kg^{-1}$ clay) | = | 5.62 | +0.59 | × FS1 | | | | |
| log Gibbsite (g $kg^{-1}$ clay) | = | 4.75 | −0.51 | × FS1 | −0.94 | × FS2 | 0.70 | × FS3 |
| log (Gibbsite/kaolin) (mol/mol) | = | 0.34 | −1.41 | × FS1 | −1.02 | × FS2 | | |

The factor was not included in the regression analysis when a coefficient was not significant at $P < 0.05$.
$Al_o$, $Fe_o$, $Si_o$: acid oxalate extractable Al, Fe, Si; $Al_p$, $Fe_p$: pyrophosphate extractable Al, Fe; $Fe_d$: Dithionite-citrate extractable Fe.
$Al_o$ − $Al_p$ and $Fe_o$ − $Fe_p$ are derived predominantly from short-range-order minerals. $Fe_o$/$Fe_d$ is an index of Fe (hydr)oxide activity. $Al_p$/$Al_o$ indicates organo-Al contribution to the active Al fraction. Kaolin and gibbsite contents were determined by DTA.
$Fe_d$, $Al_p$/$Al_o$ and $Si_o$/($Al_o$ − $Al_p$)were not significantly regressed with the factor scores.

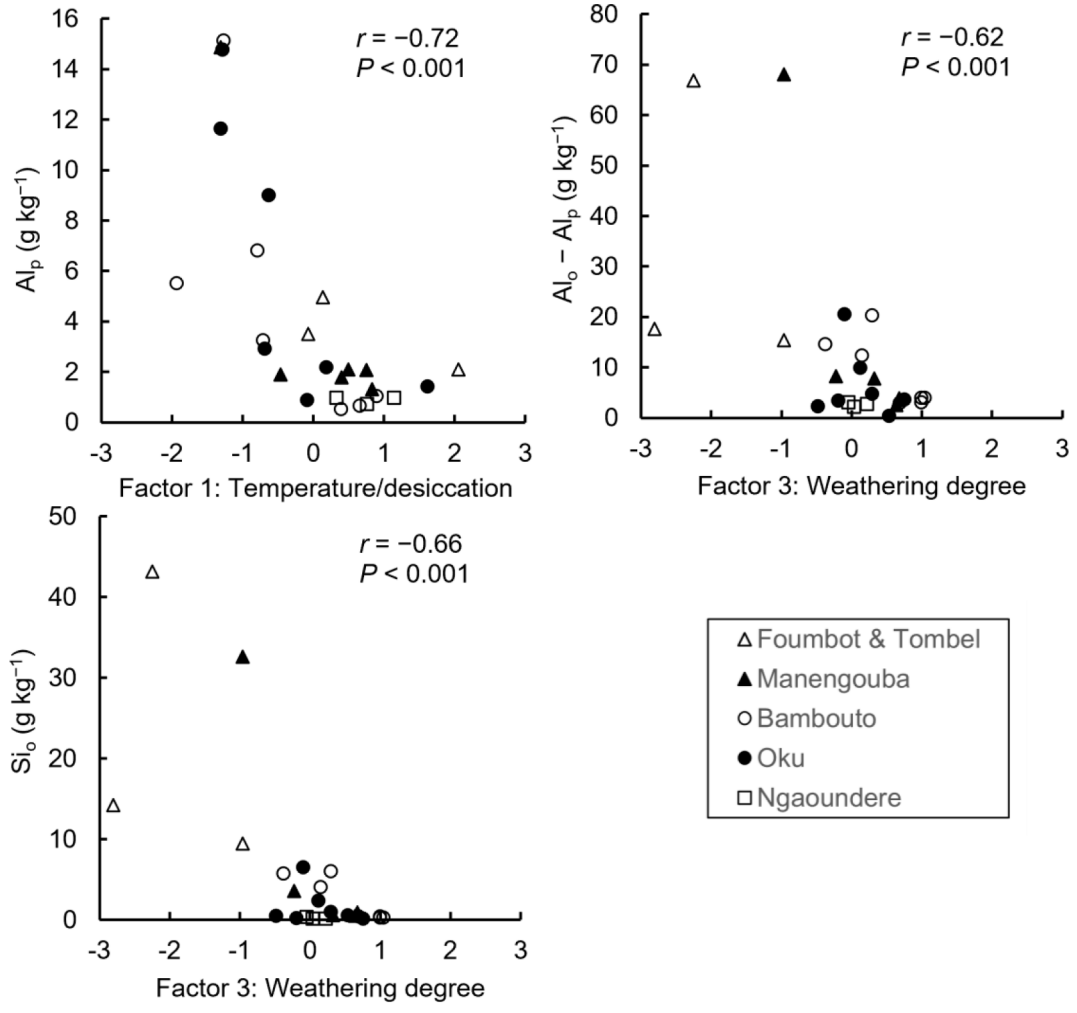


**Fig. 3.** Relationships between temperature/desiccation factor vs organo-Al complexes ($Al_p$), weathering degree factor vs short-range-order Al ($Al_o$ − $Al_p$), and weathering degree vs short-range-order Si ($Si_o$) for B horizons.

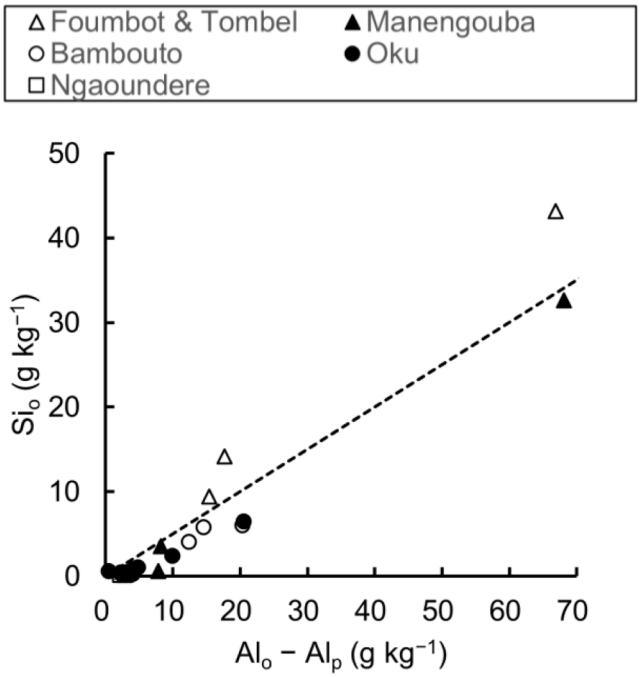


**Fig. 4.** Relationship between short-range-order Al ($Al_o - Al_p$) and Si ($Si_o$) for B horizons. Dashed line indicates a Si:Al molar ratio of 1:2.

$-0.48$, $P < 0.05$ and $r = 0.50$, $P < 0.01$, respectively), whereas gibbsite content had no correlation with kaolin minerals (Fig. S4).

## 4. Discussion

### 4.1. Parent material, climate and weathering degree

Parent materials of the studied soils were all considered to be of basaltic composition, as reported in Dongmo et al. (2010) and Marzoli et al. (2000) and supported by consistently high total Fe contents with some variability in base-element concentrations (Table 2). The free Fe (hydr)oxide content indicated by $Fe_d$ was high (>~80 g $kg^{-1}$) and increased with weathering (Table 6). Since Fe is relatively immobile in well-drained soils, it becomes enriched as other more mobile elements (e.g., Si, Ca, Mg, K, and Na) are leached as part of the weathering process. Hydroxy-Al interlayered vermiculite and quartz were found in most soils as minor constituents (Table 8). Mica, the precursor of hydroxy-Al interlayered vermiculite, and quartz are generally not found in parent materials of basaltic composition. Therefore, we posit that mica and quartz may originate from eolian dust, which is widely distributed in West Africa and a known source of quartz and 2:1 layer silicates (Dia et al., 2006; Mizota et al., 1996).

Temperature and moisture conditions varied widely among the soils within our study area. Factor 1 of the PCA analysis incorporates temperature differences along the elevational gradients, as well as the intensity of desiccation during the dry season (Table 4). Factor 1 also includes loading from organic C content, which responds sensitively to temperature along most elevational gradients (Lyu et al., 2021; Rial et al., 2017; Tsai et al., 2010). Moreover, climate was also expressed in a precipitation/leaching component (Factor 2) that was highest in the coastal regions (Tombel graben and Manengouba) and progressively decreased inland to the Ngaoundere plateau, reflecting the regional precipitation gradient (Fig. S1).

The soils at Foumbot and Tombel graben (coastal region) were less weathered Andisols, whereas the soils at the Ngaoundere plateau (inland region) were highly weathered to Oxisols. This geographical distribution in the degree of soil weathering is clearly reflected in factor 3 (Table 4, Fig. 2a), which further manifests in soil age (i.e., how long weathering has occurred). For example, the TRB value, which indicates the content of weatherable minerals (IUSS Working Group WRB, 2015), was high (>100 $cmol_c$ $kg^{-1}$) in the soils from Foumbot and Tombel graben and some soils at Mount Manengouba (Table 2 and Table S2). Similarly, the desilication metric, $Si_t/(Al_t + Fe_t)$, was high in soils with higher TRB values (Fig. S4). The younger, coastal region soils had low factor 3 scores, whereas the older, inland soils were more weathered and had similar TRB values (Table 2 and Table S2) and factor 3 scores (Fig. 2a). Among the more inland soils, the soils at Mount Oku had relatively high TRB values (>50 $cmol_c$ $kg^{-1}$, Table S2), which may result from the drier climate of the region. However, the soils from the Ngaoundere plateau also formed under drier conditions, but had lower TRB values (<50 $cmol_c$ $kg^{-1}$, Table. S2), as well as low CEC values (Table 3). These results infer that the Ngaoundere soils have experienced the strongest weathering among the studied soils, which is most likely associated with their considerably greater age.

### 4.2. Effect of temperature on active Al and Fe contents

Lower temperatures were associated with a higher active Al ($Al_o$) content, especially the organo-Al complex ($Al_p$) fraction that represents a portion of $Al_o$. High $Al_o$ and $Al_p$ were found in soils under low-temperature conditions (Tables 6 and 7, Fig. 3), and $Al_p$ was strongly correlated with total C. The higher $Al_o$ contents at lower temperatures appear to originate primarily from the formation of organo-Al complexes ($Al_p$) rather than SRO minerals ($Al_o - Al_p$), which did not correlate with the temperature/desiccation intensity factor (Table 6). Low temperature retards the decomposition of organic matter and increases its opportunity to form complexes with Al (Caner et al., 2000; Lyu et al., 2022; Van Ranst et al., 2019a). Similarly, the formation of organo-Fe complexes was indicated by $Fe_p$ values. There was a negative relationship between the temperature/desiccation intensity factor and $Fe_p$ (Tables 6 and 7), and a positive correlation between $Fe_p$ and total C (Fig. S4).

Several studies posit that chemical stabilization of soil organic matter via formation of Al/Fe–humus complexes is an important process for organic matter accumulation in Andisols (e.g., Baldock and Skjemstad, 2000; Egashira et al., 1997; Percival et al., 2000). Organo-Al complexes tend to be predominant at pH values of 5 or less (Takahashi and Dahlgren, 2016), whereby $Al^{3+}$ solubility increases exponentially providing plentiful $Al^{3+}$ to participate in complexation reactions with organic ligands. However, $Al_p/Al_o$ was not correlated with pH in the studied soils (Fig. S4), probably because pH values <5 were only found for the older soils from Ngaoundere plateau and low elevation areas near Mount Manengouba (Table 3 and Table S2). These latter soils had low $Al_o$ and $Al_p$ values that we ascribe to the higher temperature that enhances the formation of crystalline minerals at the expense of organo-metal complexes and SRO minerals, as reported for Hawaiian basalt soils (Chorover et al. 2004).

Notably, a negative correlation between $Al_o$ and temperature was also found for soils from the non-volcanic regions of Cameroon ($r = -0.33$, $P < 0.05$; Fig. S6). Importantly, this finding indicates that low temperature contributes to the formation of active Al not only in soils of volcanic origin, but also in non-volcanic soils (Caner et al., 2000). However, $Al_o$ values were relatively low (<6 g $kg^{-1}$, Fig. S6) in the non-volcanic soils, hence these non-volcanic soils do not meet andic soil properties based on the $Al_o + 1/2\ Fe_o$ criterion of ≥20 g $kg^{-1}$. One reason for these low active Al values may result from the lack of non-volcanic soils with low temperatures (<22 °C), which cannot be found in Cameroon except for volcanic regions (Fig. 1). Though we need to further examine the extent to which low temperature contributes to $Al_o$ content, considering that $Al_o$ values are generally low in non-volcanic soils of temperate regions, the effects might be limited.

In contrast to $Al_o$, no effect of temperature was found for the $Fe_o$ and $Si_o$ contents of the non-volcanic soils in Cameroon. The lack of a relationship with temperature possibly results from $Fe^{3+}$ in (hydr)oxides

**Table 8**
Mineralogical composition of B horizons.

| Site | Selective dissolution | | X-ray diffraction [a] | | | | | | | DTA [b] | |
|---|---|---|---|---|---|---|---|---|---|---|---|
| | Allo [c,d] | Ferr [c] | Smec [c] | HIV [c] | Mica | Halloysite 1.0 nm | Kaolin 0.7 nm | Gibb [c] | Quartz | Kaolin | Gibb [c] |
| | ($g\ kg^{-1}$) | | | | | | | | | ($g\ kg_{clay}^{-1}$) | |
| Foumbot & Tombel graben | | | | | | | | | | | |
| F1 | 77 | 35 | − | − | − | − | − | − | + | 614 | 74 |
| T1 | 265 | 85 | − | − | − | − | ++ | − | ± | 77 | 0 |
| T2 | 60 | 46 | − | − | − | + | + | + | ± | 394 | 10 |
| Mount Manengouba | | | | | | | | | | | |
| M1 | 262 | 97 | − | + | − | − | + | + | + | 10 | 77 |
| M2 | 32 | 42 | − | − | − | + | + | + | ± | 481 | 40 |
| M3 | | 15 | − | ± | ± | − | ++ | + | + | 648 | 59 |
| M4 | | 29 | − | ± | ± | − | ++ | − | + | 562 | 2 |
| M5 | | 16 | − | ± | − | − | ++ | ± | + | 602 | 1 |
| M6 | | 8 | − | ± | ± | − | ++ | + | + | 572 | 34 |
| Mount Bambouto | | | | | | | | | | | |
| B1 | 97 | 38 | − | − | − | − | ± | + | + | 26 | 293 |
| B2 | 55 | 38 | − | + | − | − | + | ++ | + | 31 | 242 |
| B3 | | 11 | − | + | − | − | + | + | + | 203 | 312 |
| B4 | 59 | 15 | − | − | − | − | + | ++ | + | 204 | 317 |
| B5 | | 7 | − | − | − | − | + | + | + | 296 | 392 |
| B6 | | 12 | − | + | − | − | + | + | ± | 388 | 221 |
| B7 | | 6 | − | ± | − | − | ++ | + | + | 435 | 189 |
| Mount Oku | | | | | | | | | | | |
| O1 | | 34 | + | + | − | − | + | + | + | 409 | 66 |
| O2 | 93 | 38 | n.d. | n.d. | n.d. | n.d. | n.d. | n.d. | n.d. | 20 | 197 |
| O3 | | 11 | − | ± | − | − | + | + | + | 166 | 388 |
| O4 | 56 | 33 | − | + | − | − | + | + | + | 46 | 293 |
| O5 | | 8 | − | − | − | − | + | ++ | + | 254 | 327 |
| O6 | | 21 | − | + | ± | − | + | + | + | 275 | 221 |
| O7 | | 10 | − | ± | − | − | ++ | + | + | 510 | 96 |
| Ngaoundere plateau | | | | | | | | | | | |
| N1 | | 7 | − | + | − | − | + | + | ± | 70 | 367 |
| N2 | | 6 | − | ± | − | − | ++ | + | − | 410 | 52 |
| N3 | | 5 | − | ± | − | − | ++ | + | − | 413 | 123 |

[a] ++: very clear, +: clear, ±: unclear, −: not detected, n.d.: not determined.
[b] DTA: differential thermal analysis.
[c] Allo: allophane, Ferr: ferrihydrite, Smec: smectite, Gibb: gibbsite, HIV: hydroxy-Al interlayered vermiculite.
[d] Calculated for soils with $Si_o > 2\ g\ kg^{-1}$.

being considered more thermodynamically stable than in the organo-Fe fraction (Ugolini and Dahlgren, 2002; Wada and Higashi, 1976). Furthermore, allophane and imogolite, as a source of $Si_o$, are generally not formed in non-volcanic soils due to the absence of rapid weathering associated with volcanic glass, which favors formation of metastable SRO minerals (Dahlgren et al., 2004).

Aluminum released by weathering demonstrated a propensity to preferentially form kaolin minerals under high-temperature conditions at lower elevations across our study sites. The $Al_o$ and $Al_p$ displayed negative correlations with kaolin minerals ($rs = -0.48$, $P < 0.05$ and $r = -0.50$, $P < 0.01$, respectively), with more kaolin found under higher temperature conditions (Tables 6 and 7). On the other hand, gibbsite is usually found in more highly weathered and leached environments that lead to desilication of soils. Gibbsite did not correlate with $Al_o$ or $Al_p$, but all of these Al phases (i.e., gibbsite, $Al_o$ and $Al_p$) were more prevalent in soils with lower temperatures at high elevations (Tables 5 and 6). Gibbsite tends to form under low silicic acid activity (Huang et al., 2002) at high elevation sites that experience continuous EP/leaching with a less intense dry season that limits seasonally high silicic acid activity during periods of desiccation (Table 1). However, organic acids may hinder the formation of crystalline $Al(OH)_3$ (gibbsite), thereby promoting the formation of organo-Al complexes (Huang et al., 2002). Gibbsite may be a source of $Al_o$ and $Al_p$, or it may co-exist in a simultaneous equilibrium with hydroxy-Al interlayers, allophanic materials and organo-Al complexes (Dahlgren et al., 2004). Competition for Al between gibbsite and hydroxy-Al interlayers of 2:1 layers (anti-gibbsite effect; Barnhisel and Bertsch, 1989; Jackson, 1963), allophane/imogolite and hydroxy-Al interlayers of 2:1 layers (anti-allophanic effect; Shoji et al., 1993), and allophane/imogolite and organic matter (Takahashi and Dahlgren, 2016) have been postulated to explain the preferential formation of various clay minerals owing to competition for available $Al^{3+}$; these relationships were not clear in the studied Cameroon soils. Given that kaolins were positively correlated to factor 1 (temperature/desiccation intensity), whereas gibbsite was negatively correlated with factor 1, it appears that kaolin and gibbsite compete for Al released by weathering, with the silicic acid activity determining the dominant weathering product.

### 4.3. Effects of weathering degree on active Al and Fe contents

Active Al/Fe ($Al_o$ and $Fe_o$) were high in the B horizons of less weathered soils (Table 6), with SRO minerals generally being the dominant form. Negative relationships between $Fe_o/Fe_d$ and the weathering factor (Tables 6 and 7) indicate progressive crystallization of Fe (hydr)oxides as the age increases from 0.12 to 0.01 Ma in Tombel graben to 11–7 Ma in Ngaoundere plateau (Dongmo et al., 2010; Enang

et al., 2020; Marzoli et al., 2000). Indicators of SRO minerals, that is $Al_o - Al_p$, $Fe_o - Fe_p$ and $Si_o$, were negatively correlated with the weathering factor score (Factor 3; Fig. 3). The greater coefficients for factor 3 scores in the regression equations (Table 7) highlight the relative importance of weathering degree on formation of SRO minerals. The high $Al_o - Al_p$, $Fe_o - Fe_p$ and $Si_o$ values were more pronounced in the younger and less weathered soils of Foumbot, Tombel graben and Mount Manengouba (Fig. 4 and Table 5). These results indicate that SRO minerals form and persist as metastable phases in the less weathered soils. Conversely, indicators of organo-Al/Fe complexes ($Al_p$ and $Fe_p$) were not correlated with the weathering factor (Table 6), suggesting that $Al_p$ and $Fe_p$ were more strongly controlled by the temperature/desiccation intensity factor through its influence on soil organic matter concentrations.

A $Si_o$ content over ~2 g $kg^{-1}$ is often a good indicator for the presence of SRO aluminosilicates in soils with volcanic parent materials (Dahlgren, 1994; Hirai et al., 1991). The $Si_o$ was strongly correlated with $Al_o - Al_p$ ($rs = 0.81$, $P < 0.001$), and the $Si_o/(Al_o - Al_p)$ ratio was close to 1:2 (Fig. 4), which is the theoretical Si:Al ratio of imogolite and Al-rich allophane (Harsh et al., 2002). These results indicate the presence of SRO aluminosilicate minerals (e.g., Al-rich allophane and/or imogolite). Negative relationships of $Si_o$ and $Si_o/(Al_o - Al_p)$ with the weathering factor (Tables 6 and 7, Fig. 3) indicate the disappearance of allophanic materials with increased weathering. Furthermore, $Si_o$ was correlated with $Fe_o - Fe_p$ ($rs = 0.81$, $P < 0.001$), suggesting inhibition of Fe (hydr)oxide crystallization by silicic acid sorption to Fe (hydr)oxides surfaces, thereby blocking precipitation sites to form a crystalline structure (Anderson and Benjamin, 1985; Churchman and Lowe, 2012). The $Fe_o - Fe_p$ fraction is often considered a measure of the ferrihydrite content (Parfitt and Childs, 1988), which exists in various states of crystallization (e.g., 2-line vs 6-line structures via XRD).

Hirai et al. (1991) proposed a $Si_o$ value of 2 g $kg^{-1}$ to distinguish volcanic ash-influenced soils from non-volcanic ash soils in Japan. For example, most volcanic soils had $Si_o$ values exceeding 2 g $kg^{-1}$, whereas brown forest soils had lower values. The $Si_o$ (2 g $kg^{-1}$) metric is likely associated with the presence versus absence of highly weatherable components comprising volcanic ejecta, such as volcanic glass. In the present study, soils having $Si_o$>2 g $kg^{-1}$ also had higher $Al_o - Al_p$ and $Fe_o - Fe_p$ values (Fig. 4), inferring an influence of tephra that preferentially weathers to SRO minerals. This residual effect of tephra parent material was not only found in the youngest volcanic soils of Tombel graben, Foumbot and Manengouba, but also in the older volcanic soils at higher elevations of Mounts Bambouto and Oku (Fig. 4).

The above mentioned influence of tephra on active Al/Fe contents sharply contrasts with the proposal that gibbsite and goethite were the primary sources of organo-Al/Fe complexes in Mount Bambouto (Van Ranst et al., 2019a; Van Ranst et al., 2019b). The higher solubility, lower thermodynamic stability and high specific surface areas of SRO minerals versus crystalline Fe and Al (hydr)oxides (Bigham et al., 2002; Harsh et al., 2002; Huang et al., 2002; Schwertmann, 2008) support the consideration that SRO minerals (allophane, imogolite, and ferrihydrite) are more important sources of Al/Fe for incorporation into organo-metal complexes as opposed to gibbsite and goethite. The Al/Fe complexed with organic matter at Mounts Bambouto and Oku may originate directly from weathering of the parent material and/or dissolution of SRO or crystalline minerals. $Si_o$ positively correlated with $Al_p$ and $Fe_p$ ($r = 0.66$, $P < 0.001$ and $r = 0.41$, $P < 0.05$, respectively) and $Si_o$ values of 2 g $kg^{-1}$ coincide with high $Al_p$ and $Fe_p$ values (Table 5), indicating simultaneous occurrence of allophanic materials and organo-Al/Fe complexes. In young tephra deposits, Al/Fe released by weathering preferentially accumulates as organo-metal complexes (Dahlgren et al., 1997; Lilienfein et al., 2003) until organic matter stocks reach a steady state with respect to organic matter input–output (plant additions versus decomposition losses). The $Al_o$ fraction in soils with allophanic materials can be quickly converted to $Al_p$ due to acidification, such as occurs in tea plantations (Anda and Dahlgren, 2020; Takahashi et al., 2008), or the addition of new organic matter via reforestation (Hunziker et al., 2019). However, neither $Al_p/Al_o$ nor $Al_p$ correlated with pH (Fig. S4), probably because of the higher pH range of the studied soils (Mostly pH > 5, Table 3 and Table S2). Considering $Al_p/Al_o$ increased with weathering (Table 6), dissolution of allophanic materials and conversion of released $Al^{3+}$ to organo-Al complexes is posited to have occurred over time.

### 4.4. Effects of precipitation and leaching on active Al and Fe contents

High precipitation/leaching may contribute to formation and persistence of active Al and Fe components. Greater $Al_o$, $Fe_o$ and $Si_o$ contents and higher $Fe_o/Fe_d$ were found in soils with higher precipitation/leaching factor scores (Factor 2; Table 6). This result is consistent with volcanic soils in a drier area of Tanzania and the Galapagos islands, where SRO minerals were less abundant in areas with low EP (Candra et al., 2019; Candra et al., 2021; Lyu et al., 2018). SRO minerals formed preferentially in areas with high leaching (Tsai et al., 2010), and drier conditions may enhance the formation of more crystalline minerals (Candra et al., 2021; Lyu et al., 2018; Rasmussen et al., 2010). Plentiful year-long soil moisture (i.e., udic) coupled with the warm temperatures (isothermic) results in rapid chemical weathering in Cameroon, which kinetically favors formation of metastable SRO minerals (Dahlgren et al., 2004; Stumm, 1992). Further, the lack of a distinct dry season hinders the crystallization process as Ostwald ripening (dissolution and reprecipitation) and dehydration are energetically and kinetically favored by prolonged periods of high temperature and desiccation (Takahashi et al., 1993; Ziegler et al., 2003). In contrast, the influence of high precipitation/leaching on organo-Al/Fe complexes was not found (Tables 6 and 7). Although high precipitation increases NPP (Del Grosso et al., 2008) and organic matter input into the soil, temperature seems to have a stronger effect in controlling microbial decomposition of organic matter in the studied soils.

The gibbsite/kaolin ratio did not increase and $Si_o/(Al_o - Al_p)$ did not decrease with the precipitation/leaching factor (Factor 2) though we expected high leaching would lead to desilication of soils and formation of Al-rich allophane and a high gibbsite/kaolin ratio as reported for other tropical regions (Churchman and Lowe, 2012; Lyu et al. 2022; Watanabe et al., 2017). Moreover, the desilicated clay mineral, gibbsite, was less abundant and the gibbsite/kaolin ratio was low in the soils with high precipitation/leaching scores (Factor 2) of the coastal region (Tombel graven and Manengouba; Table 6, Fig. 2b). Because soils in the coastal region received more recent volcanic tephra, desilication would be insufficient to promote gibbsite formation (Table 2), although the weathering factor (Factor 3) was not significantly different (Fig. 2a). Over time kaolin minerals would be replaced by gibbsite as was found in more weathered soils in Mount Banbouto, Mount Oku and Ngaoundere plateau (Table 8). Similarly, the effect of leaching lowering the $Si_o/(Al_o - Al_p)$ ratio may be diminished by a greater supply of Si from the less weathered, kaolin-dominant soils of the coastal region.

### 4.5. Soil genesis progression in the Cameroon volcanic line

The taxonomic classification of the soils reflects the observed clay mineralogy and suggests the progression from Entisols → Andisols → Inceptisols → Ultisols/Alfisols → Oxisols along the Cameroon volcanic line. This sequence is similar to those found in humid volcanic regions with andesitic/basaltic parent materials (Chorover et al., 1999; Nieuwenhuyse and van Breemen, 1997; Rasmussen et al., 2007; Tsai et al., 2010). Entisols are found on the recent volcanic materials above the tree line of Mont Cameroon, whereas Andisols are distributed below tree line (Proctor et al., 2007). Andisols are also found near volcanic cones in the coastal region (Delvaux et al., 1989), as we found in this study. An Andisols → Inceptisols → Ultisols sequence was found in Mounts Manengouba, Banbouto and Oku, where more developed soils were found at lower elevations. The transition of Andisols to Inceptisols occurs during the transformation of SRO to crystalline clay minerals, which allows for enhanced clay translocation to form an argillic horizon (Alfisols/

Ultisols) as crystalline clays are more dispersible than SRO minerals, such as allophanic materials. Alfisols can be an alternative to Ultisols if base saturation is sufficient (Delvaux et al., 1989; Van Ranst et al., 2019a). More weathered Oxisols were found on the Ngaoundere plateau and lower elevations of Banbouto.

## 5. Conclusion

Our analysis revealed factors controlling active Al and Fe ($Al_o$ and $Fe_o$) forms and abundances in tropical volcanic soils along the Cameroon volcanic line having wide ranges of temperature, moisture and weathering degree. Organo-Al/Fe complexes and SRO minerals were controlled by different factors. Organo-Al/Fe complexes ($Al_p$ and $Fe_p$) were high under low-temperature conditions owing to the low organic matter decomposition rate and its association with Al and Fe. The formation of organo-Al complexes under lower temperatures was also confirmed for the non-volcanic soil regions of Cameroon. Conversely, SRO minerals, indicated by $Si_o$, $Al_o - Al_p$ and $Fe_o - Fe_p$, were high in less weathered soils where the rapid weathering of tephra (especially the volcanic glass) presumably provides a higher supply of Si, Al and Fe. Furthermore, high precipitation/leaching contributed to the formation and preservation of active Al and Fe. Although the low temperature contributes to higher $Al_p$ and $Fe_p$, and thus $Al_o$ and $Fe_o$, their values were positively correlated with $Si_o$ and not with gibbsite and free Fe (hydr) oxides ($Fe_d$), inferring that the organo-Al/Fe complexes formed directly from weathering of volcanic tephra and/or SRO minerals rather than crystalline Al and Fe (hydr)oxides. A $Si_o$ value of $\sim 2$ g $kg^{-1}$ appeared to effectively distinguish soils with prominent SRO mineral contents, and thereby provides a metric to identify soils that retain an influence of volcanic parent materials on the active Al and Fe fraction.

## Declaration of Competing Interest

The authors declare the following financial interests/personal relationships which may be considered as potential competing interests:

Tetsuhiro Watanabe reports financial support was provided by Japan Society for the Promotion of Science. Shinya Funakawa reports financial support was provided by Japan Society for the Promotion of Science. Atsushi Nakao reports a relationship with Japan Society for the Promotion of Science that includes: funding grants.

The remaining authors declare that they have no known competing financial interests or personal relationships that could have appeared to influence the work reported in this paper.

## Data availability

Data will be made available on request.

## Acknowledgments

This work was supported by the JSPS KAKENHI Grant Numbers 17H06171, 18H02314, 20H04322, and 20KK0261.

## Appendix A. Supplementary data

Supplementary data to this article can be found online at https://doi.org/10.1016/j.geoderma.2022.116289.

## References

Anda, M., Dahlgren, R.A., 2020. Mineralogical and surface charge characteristics of Andosols experiencing long-term, land-use change in West Java, Indonesia. Soil Sci. Plant Nutr. 66 (5), 702–713.
Anderson, P.R., Benjamin, M.M., 1985. Effects of silicon on the crystallization and adsorption properties of ferric oxides. Environ. Sci. Technol. 19 (11), 1048–1053.
Asano, M., Wagai, R., 2014. Evidence of aggregate hierarchy at micro- to submicron scales in an allophanic Andisol. Geoderma 216, 62–74.
Ashida, K., Watanabe, T., Urayama, S., Hartono, A., Kilasara, M., Ze, A.D.M., Nakao, A., Sugihara, S., Funakawa, S., 2021. Quantitative relationship between organic carbon and geochemical properties in tropical surface and subsurface soils. Biogeochemistry 155 (1), 77–95.
Baldock, J.A., Skjemstad, J.O., 2000. Role of the soil matrix and minerals in protecting natural organic materials against biological attack. Org. Geochem. 31 (7–8), 697–710.
Barnhisel, I.B., Bertsch, P.M., 1989. Chlorites and hydroxy-interlayered vermiculite and smectite. In: Dixon, J.B., Weed, S.B. (Eds.), Minerals in Soil Environments. SSSA, Madison, WI, pp. 729–788.
Best, M.G., 2003. Igneous and Metamorphic Petrology, 2nd ed. Blackwell, Massachusetts, USA.
Bigham, J.M., Fitzpatrick, R.W., Schulze, D.G., 2002. Iron oxides. In: Dixon, J.B., Schulze, D.G. (Eds.), Soil Mineralogy With Environmental Applications. SSSA, Madison, WI, pp. 323–366.
Blakemore, L.C., Searle, P.L., Daly, B.K., 1987. Methods for chemical analysis of soils. New Zealand Soil Bureau Scientific Report 10A. DSIR, New Zealand.
Candra, I.N., Gerzabek, M.H., Ottner, F., Tintner, J., Wriessnig, K., Zehetner, F., 2019. Weathering and soil formation in rhyolitic tephra along a moisture gradient on Alcedo Volcano, Galapagos. Geoderma 343, 215–225.
Candra, I.N., Gerzabek, M.H., Ottner, F., Wriessnig, K., Tintner, J., Schmidt, G., Rechberger, M.V., Rampazzo, N., Zehetner, F., 2021. Soil development and mineral transformations along a one-million-year chronosequence on the Galapagos Islands. Soil Sci. Soc. Am. J. 85 (6), 2077–2099.
Caner, L., Bourgeon, G., Toutain, F., Herbillon, A.J., 2000. Characteristics of non-allophanic Andisols derived from low-activity clay regoliths in the Nilgiri Hills (Southern India). Eur. J. Soil Sci. 51 (4), 553–563.
Childs, C.W., 1985. Towards understanding soil mineralogy II. Notes on ferrihydrite. N.Z. Soil Bureau Laboratory Report CM7. Department of Scientific and Industrial Research.
Chorover, J., DiChiaro, M.J., Chadwick, O.A., 1999. Structural charge and cesium retention in a chronosequence of tephritic soils. Soil Sci. Soc. Am. J. 63 (1), 169–177.
Chorover, J., Amistadi, M.K., Chadwick, O.A., 2004. Surface charge evolution of mineral-organic complexes during pedogenesis in Hawaiian basalt. Geochim. Cosmochim. Acta 68 (23), 4859–4876.
Churchman, G.J., Lowe, D.J., 2012. Alteration, formation, and occurrence of minerals in soils. In: Huang, P.M., Li, Y., Sumner, M.E. (Eds.), Handbook of Soil Science Properties and Processes. CRC Press, Boca Raton, FL.
Dahlgren, R., 1994. Quantification of Allophane and Imogolite. In: Amonette, J.E., Stucki, J.W. (Eds.), Quantitative Methods in Soil Mineralogy. Soil Science of America Inc, Madison, WI, USA, pp. 430–451.
Dahlgren, R.A., Dragoo, J.P., Ugolini, F.C., 1997. Weathering of Mt. St. Helens tephra under a cryic-udic climatic regime. Soil Sci. Soc. Am. J. 61 (5), 1519–1525.
Dahlgren, R.A., Saigusa, M., Ugolini, F.C., 2004. The nature, properties and management of volcanic soils. Adv. Agron. 82, 113–182.
Del Grosso, S., Parton, W., Stohlgren, T., Zheng, D.L., Bachelet, D., Prince, S., Hibbard, K., Olson, R., 2008. Global potential net primary production predicted from vegetation class, precipitation, and temperature. Ecology 89 (8), 2117–2126.
Delvaux, B., Herbillon, A.J., Vielvoye, L., 1989. Characterization of a weathering sequence of soils derived from volcanic ash in Cameroon - taxonomic, mineralogical and agronomic implications. Geoderma 45 (3–4), 375–388.
Dia, A., Chauvel, C., Bulourde, M., Gerard, M., 2006. Eolian contribution to soils on Mount Cameroon: isotopic and trace element records. Chem. Geol. 226 (3–4), 232–252.
Dongmo, A.K., Nkouathio, D., Pouclet, A., Bardintzeff, J.M., Wandji, P., Nono, A., Guillou, H., 2010. The discovery of late Quaternary basalt on Mount Bambouto: implications for recent widespread volcanic activity in the southern Cameroon Line. J. Afr. Earth Sci. 57 (1–2), 96–108.
Egashira, K., Uchida, S., Nakashima, S., 1997. Aluminum-humus complexes for accumulation of organic matter in black-colored soils under grass vegetation in Bolivia. Soil Sci. Plant Nutr. 43 (1), 25–33.
Enang, R.K., Yerima, B.P.K., Kome, G.K., Van Ranst, E., 2020. Soil physicochemical properties and geochemical indices: Diagnostic tools for evaluating pedogenesis in tephra-derived soils along the Cameroon Volcanic Line. Eurasian Soil Sci. 53 (8), 1079–1099.
Enang, R.K., Mees, F., Yerima, B.P.K., Van Ranst, E., 2021. Iddingsitisation of olivine and kaolinitisation of biotite in two contrasting tephra-derived soils along the Cameroon Volcanic Line (CVL). Soil Res. 59 (3), 276–286.
Etame, J., Gerard, M., Suh, C.E., Bilong, P., 2009. Halloysite neoformation during the weathering of nephelinitic rocks under humid tropical conditions at Mt Etinde, Cameroon. Geoderma 154 (1–2), 59–68.
Gee, G.W., Or, D., 2002. Particle-size analysis. In: Dane, J.H., Topp, G.C. (Eds.), Methods of Soil Analysis. Part 4. Physical Methods. SSSA, Madison, WI, pp. 255–293.
Harris, W., White, G.N., 2008. X-ray diffraction. In: Ulery, A.L., Drees, L.R. (Eds.), Methods of Soil Analysis Part 5 Mineralogical Methods. SSSA, Madison, WI, pp. 81–115.
Harsh, J., Chorover, J., Nizeyimana, E., 2002. Allophane and imogolite. In: Dixon, J.B., Schulze, D.G. (Eds.), Soil Mineralogy With Environmental Applications. SSSA, Madison, WI, pp. 291–322.
Hijmans, R.J., Cameron, S.E., Parra, J.L., Jones, P.G., Jarvis, A., 2005. Very high resolution interpolated climate surfaces for global land areas. Int. J. Climato. 25 (15), 1965–1978.
Hirai, H., Sakurai, K., Kyuma, K., 1991. Characteristics of brown forest soils developed under beech forests in the Kinki and the Tohoku districts with special reference to their pedogenetic processes. Soil Sci. Plant Nutr. 37 (3), 497–507.

Hossner, L.R., 1996. Dissolution for total elemental analysis. In: Sparks, D.L. (Ed.), Methods of Soil Analysis. Part 3. Chemical Methods. SSSA, Madison, WI, pp. 49–64.
Huang, P.M., Wang, M.K., Kampf, N., Schulze, D.G., 2002. Aluminum hydroxides. In: Dixon, J.B., Schulze, D.G. (Eds.), Soil Mineralogy With Environmental Applications. SSSA Book Series 7. SSSA, Madison, WI, pp. 261–289.
Hunziker, M., Arnalds, O., Kuhn, N.J., 2019. Evaluating the carbon sequestration potential of volcanic soils in southern Iceland after birch afforestation. Soil 5 (2), 223–238.
IUSS Working Group WRB, 2015. World reference base for soil resources 2014. Update 2015. World Soil Resources Reports No. 106. FAO, Rome.
Jackson, M.L., 1963. Aluminum bonding in soils: a unifying principle in soil science. Soil Sci. Soc. Am. Proc. 27 (1), 1–10.
Jones, A., Breuning-Madsen, H., Brossard, M., Dampha, A., Deckers, J., Dewitte, O., Gallali, T., Hallett, S., Jones, R., Kilasara, M., Le Roux, P., Micheli, E., Montanarella, L., Spaargaren, O., Thiombiano, L., Van Ranst, E., Yemefack, M., Zougmoré, R., 2013. Soil Atlas of Africa. European Commission, Luxembourg.
Lilienfein, J., Qualls, R.G., Uselman, S.M., Bridgham, S.D., 2003. Soil formation and organic matter accretion in a young andesitic chronosequence at Mt. Shasta, California. Geoderma 116 (3–4), 249–264.
Lyu, H., Watanabe, T., Kilasara, M., Funakawa, S., 2018. Effects of climate on distribution of soil secondary minerals in volcanic regions of Tanzania. Catena 166, 209–219.
Lyu, H., Watanabe, T., Kilasara, M., Hartono, A., Funakawa, S., 2021. Soil organic carbon pools controlled by climate and geochemistry in tropical volcanic regions. Sci. Total Environ. 761.
Lyu, H., Watanabe, T., Ota , Y., Hartono, A., Anda, M., Dahlgren, R.A., Funakawa, S., 2022. Climatic controls on soil clay mineral distributions in humid volcanic regions of Sumatra and Java, Indonesia. Geoderma (accepted).
Marzoli, A., Piccirillo, E.M., Renne, P.R., Bellieni, G., Iacumin, M., Nyobe, J.B., Tongwa, A.T., 2000. The Cameroon Volcanic Line revisited: Petrogenesis of continental basaltic magmas from lithospheric and asthenospheric mantle sources. J. Petrol. 41 (1), 87–109.
Mayaux, P., Richards, T., Janodet, E., 1999. A vegetation map of Central Africa derived from satellite imagery. J. Biogeogr. 26 (2), 353–366.
Mizota, C., Faure, K., Yamamoto, M., 1996. Provenance of quartz in sedimentary mantles and laterites overlying bedrock in West Africa: evidence from oxygen isotopes. Geoderma 72 (1–2), 65–74.
Morin, S., 1989. Hautes Terres et Bassins de l'Ouest Cameroun. Université de Yaoundé.
Nakao, A., Sugihara, S., Maejima, Y., Tsukada, H., Funakawa, S., 2017. Ferralsols in the Cameroon plateaus, with a focus on the mineralogical control on their cation exchange capacities. Geoderma 285, 206–216.
Nieuwenhuyse, A., van Breemen, N., 1997. Quantitative aspects of weathering and neoformation in selected Costa Rican volcanic soils. Soil Sci. Soc. Am. J. 61 (5), 1450–1458.
Nkouathio, D.G., Dongmo, A.K., Bardintzeff, J.M., Wandji, P., Bellon, H., Pouclet, A., 2008. Evolution of volcanism in graben and horst structures along the Cenozoic Cameroon Line (Africa): Implications for tectonic evolution and mantle source composition. Mineral. Petrol. 94 (3–4), 287–303.
Parfitt, R.L., 1990. Allophane in New Zealand—A review. Aust. J. Soil Res. 28 (3), 343–360.
Parfitt, R.L., Childs, C.W., 1988. Estimation of forms of Fe and Al: a review, and analysis of contrasting soils by dissolution and Mössbauer methods. Aust. J. Soil Res. 26 (1), 121–144.
Parfitt, R.L., Russell, M., Orbell, G.E., 1983. Weathering sequence of soils from volcanic ash involving allophane and halloysite, New-Zealand. Geoderma 29 (1), 41–57.
Pennock, D., Yates, T., Braidek, J., 2007. Soil sampling designs. In: Carter, M.R., Gregorich, E.G. (Eds.), Soil Sampling and Methods of Analysis. CRC Press, Boca Raton, FL, pp. 1–14.
Percival, H.J., Parfitt, R.L., Scott, N.A., 2000. Factors controlling soil carbon levels in New Zealand grasslands: is clay content important? Soil Sci. Soc. Am. J. 64 (5), 1623–1630.
Proctor, J., Edwards, I.D., Payton, R.W., Nagy, L., 2007. Zonation of forest vegetation and soils of Mount Cameroon, West Africa. Plant Ecol. 192 (2), 251–269.
Rasmussen, C., Matsuyama, N., Dahlgren, R.A., Southard, R.J., Brauer, N., 2007. Soil genesis and mineral transformation across an environmental gradient on andesitic lahar. Soil Sci. Soc. Am. J. 71 (1), 225–237.
Rasmussen, C., Dahlgren, R.A., Southard, R.J., 2010. Basalt weathering and pedogenesis across an environmental gradient in the southern Cascade Range, California, USA. Geoderma 154 (3–4), 473–485.
Rennert, T., 2019. Wet-chemical extractions to characterise pedogenic Al and Fe species - a critical review. Soil Res. 57 (1), 1–16.
Rial, M., Cortizas, A.M., Taboada, T., Rodriguez-Lado, L., 2017. Soil organic carbon stocks in Santa Cruz Island, Galapagos, under different climate change scenarios. Catena 156, 74–81.
Schuppli, P.A., Ross, G.J., McKeague, J.A., 1983. The effective removal of suspended materials from pyrophosphate extracts of soils from tropical and temperate regions. Soil Sci. Soc. Am. J. 47 (5), 1026–1032.
Schwertmann, U., 1985. The effect of pedogenic environments on iron oxide minerals. In: Stewart, B.A. (Ed.), Advances in Soil Science. Springer-Verlag, New York, pp. 171–200.
Schwertmann, U., 2008. Iron oxides. In: Chesworth, W. (Ed.), Encyclopedia of Soil Science. Springer, pp. 363–369.
Shang, C., Zelazny, L., 2008. Selective dissolution techniques for mineral analysis of soils and sediments. In: Ulery, A.L., Drees, L.R. (Eds.), Methods of Soil Analysis Part 5 Mineralogical Methods. Soil Science Society of America Inc, Madison, Wisconsin, USA, pp. 33–80.
Shoji, S., Nanzyo, M., Dahlgren, R., 1993. Volcanic ash soils—genesis, properties and utilization. Development in Soil Science. Elsevier, Amsterdam.
Soil Survey Staff, 1999. Soil Taxonomy, 2nd ed. USDA-NRCS, Washington, DC.
Soil Survey Staff, 2014. Keys to Soil Taxonomy, 12th ed. USDA-NRCS, Washington, DC.
Soil Survey Staff, 1996. Soil survey laboratory methods manual. Soil Survey Investigations Report No. 42 Version 3.0. USDA-NRCS, Washington, DC.
Stumm, W., 1992. Chemistry of the Solid–Water Interface: Processes at the Mineral–Water and Particle–Water Interface in Natural Systems. John Wiley & Sons, NJ, USA.
Takahashi, T., Dahlgren, R., van Susteren, P., 1993. Clay mineralogy and chemistry of soils formed in volcanic materials in the xeric moisture regime of northern California. Geoderma 59 (1–4), 131–150.
Takahashi, T., Dahlgren, R.A., 2016. Nature, properties and function of aluminum-humus complexes in volcanic soils. Geoderma 263, 110–121.
Takahashi, T., Mitamura, A., Ito, T., Ito, K., Nanzyo, M., Saigusa, M., 2008. Aluminum solubility of strongly acidified allophanic Andosols from Kagoshima Prefecture, southern Japan. Soil Sci. Plant Nutr. 54 (3), 362–368.
Tematio, P., Kengni, L., Bitom, D., Hodson, M., Fopoussi, J.C., Leumbe, O., Mpakam, H. G., Tsozue, D., 2004. Soils and their distribution on Bambouto volcanic mountain, west Cameroon highland, central Africa. J. Afr. Earth Sci. 39 (3–5), 447–457.
Thornthwaite, C.W., 1948. An approach toward a rational classification of climate. Geogr. Rev. 38, 55–94.
Torn, M.S., Trumbore, S.E., Chadwick, O.A., Vitousek, P.M., Hendricks, D.M., 1997. Mineral control of soil organic carbon storage and turnover. Nature 389, 170–173.
Tsai, C.C., Chen, Z.S., Kao, C.I., Ottner, F., Kao, S.J., Zehetner, F., 2010. Pedogenic development of volcanic ash soils along a climosequence in Northern Taiwan. Geoderma 156 (1–2), 48–59.
Ugolini, F.C., Dahlgren, R.A., 2002. Soil development in volcanic ash. Glob. Environ. Res. 6 (2), 69–81.
Van Ranst, E., Doube, M., Mees, F., Dumon, M., Ye, L., Delvaux, B., 2019a. Andosolization of ferrallitic soils in the Bambouto Mountains, West Cameroon. Geoderma 340, 81–93.
Van Ranst, E., Mees, F., De Grave, E., Ye, L., Cornelis, J.T., Delvaux, B., 2019b. Impact of andosolization on pedogenic Fe oxides in ferrallitic soils. Geoderma 347, 244–251.
Wada, K., Higashi, T., 1976. The categories of aluminium- and iron-humus complexes in Ando soils determined by selective dissolution. J. Soil Sci. 27 (3), 357–368.
Watanabe, T., Hase, E., Funakawa, S., Kosaki, T., 2015. Inhibitory effect of soil micropores and small mesopores on phosphate extraction from soils. Soil Sci. 180 (3), 97–106.
Watanabe, T., Hasenaka, Y., Hartono, A., Sabiham, S., Nakao, A., Funakawa, S., 2017. Parent materials and climate control secondary mineral distributions in soils of Kalimantan, Indonesia. Soil Sci. Soc. Am. J. 81 (1), 124–137.
Yerima, B.P.K., Van Ranst, E., 2005. The physical environment and factors of soil formation in Cameroon. In: Trafford, B.C. (Ed.), Major Soil Classification Systems Used in the Tropics: Soils of Cameroon. Canada, pp. 102–149.
Ziegler, K., Hsieh, J.C.C., Chadwick, O.A., Kelly, E.F., Hendricks, D.M., Savin, S.M., 2003. Halloysite as a kinetically controlled end product of arid-zone basalt weathering. Chem. Geol. 202, 461–478.